Ore Geology Reviews 101 (2018) 785–802

Contents lists available at ScienceDirect

Ore Geology Reviews

journal homepage: www.elsevier.com/locate/oregeorev

The genesis of the Dahebian Zn-Pb deposit and associated barite mineralization: Implications for hydrothermal fluid venting events along the Nanhua Basin, South China

Zhengbing Zhou[a,b,c], Hanjie Wen[b,c,*], Chaojian Qin[b], Jeffrey de Fourestier[a], Ling Liu[d], Qingpeng Shi[d]

[a] State Key Laboratory of Nuclear Resources and Environment (East China University of Technology), Nanchang 330013, PR China
[b] State Key Laboratory of Ore Deposit Geochemistry, Chinese Academy of Sciences, Guiyang 550081, PR China
[c] University of Chinese Academy of Sciences, Beijing 100049, PR China
[d] Geological Party 101, Guizhou Bureau of Geology and Minerals Exploration & Development, Kaili 556000, PR China

ARTICLE INFO

Keywords:
The Dahebian zinc-lead deposit
Stratiform barite deposit
Nanhua Basin
Sedimentary exhalative
South China

ABSTRACT

The Dahebian stratiform barite deposit, which is situated in the Nanhua Basin, is one of the world's largest and most important barite deposits. This deposit was formed through sedimentary exhalative processes in the early Cambrian stage. Recently, beneath stratiform barite ore, stratabound Zn-Pb-(Fe-bearing) sulfide mineralization, which is hosted by the Doushantuo Formation, was discovered. Ores that represent Zn-Pb sulfide mineralization are mainly discordant but stratabound. The Doushantuo Formation consists of laminated interbedded layers of micritic dolomite and carbonaceous mudstone, associated with phosphorite and chert. The sulfide ores consist primarily of sphalerite, pyrite and galena. The associated gangue minerals are barite, quartz, minor calcite, as well as trace amounts of apatite and hyalophane. Hyalophane found in the stratiform barite ore is richer in barium but poorer in potassium than that associated with the sulfide ores. This outcome corresponds to ascending hydrothermal fluids that are richer in barium along with sulfide mineralization. Investigation of the ore fluid reveals relatively high temperature (142–368 °C) with scattered salinity (0.53–25.62 wt% NaCl eq.). This finding suggests that fluid cooling and/or mixing with seawater could be the primary mechanisms that prompted the ore formation. Sulfides selected from the zinc-lead sulfide ores and stratiform barite ore have similar sulfur isotopic compositions, with $\delta^{34}S$ values ranging from 13.5‰ to 30.0‰; $\delta^{34}S$ values of barite from these ores are analogous, with $\delta^{34}S$ values ranging from 29.5‰ to 55.1‰. The sulfur isotopic fractionation between minerals (barite and sulfide) and the early Cambrian seawater is $\Delta_{Barite\text{-}Seawater} = 7.8‰$ and $\Delta_{Sulfide\text{-}Seawater} = -12.1‰$, respectively, demonstrating that the sulfur in the Dahebian zinc-lead deposit and the stratiform barite deposit were derived from the early Cambrian stratified seawater column. Lead isotopic compositions of sulfide ores indicate that these ore metals are mainly sourced from rocks of the Doushantuo Formation and the underlying fold basement.

Therefore, the Dahebian zinc-lead deposit and stratiform barite deposit probably arose from Selwyn-Type sedimentary exhalative hydrothermal fluids. Zn-Pb sulfides were mineralized in the feeder zone of these hydrothermal fluids, and the stratiform barite ore deposits represent the upper sedimentary-exhalative mineralization. This finding points to intensive Zn-Pb-Fe-Ba hydrothermal fluid venting into the Nanhua Basin and to relatively oxic deep ocean waters during the early Cambrian.

1. Introduction

The Nanhua Basin is considered an intracontinental marine basin that developed during the breakup of the Rodinia Supercontinent (Fig. 1; Wang and Li, 2003; Wang et al., 2014; Zhang et al., 2013). It is characterized by episodic hydrothermal fluid exhalative events (*e.g.*, Lott et al., 1999; Fang et al., 2002; Jiang et al., 2006a,b; Chen et al., 2009; Huang et al., 2011; Wen and Carignan, 2011; Fan et al., 2013) and long-term stratified oxic-suboxic-euxinic basins during the Neoproterozoic to early Cambrian (Li et al., 2010, 2015). Along the margin

* Corresponding author at: State Key Laboratory of Ore Deposit Geochemistry, Chinese Academy of Sciences, Guiyang 550081, PR China.
E-mail address: wenhanjie@vip.gyig.ac.cn (H. Wen).

https://doi.org/10.1016/j.oregeorev.2018.08.013
Received 14 February 2018; Received in revised form 8 August 2018; Accepted 10 August 2018
Available online 11 August 2018
0169-1368/

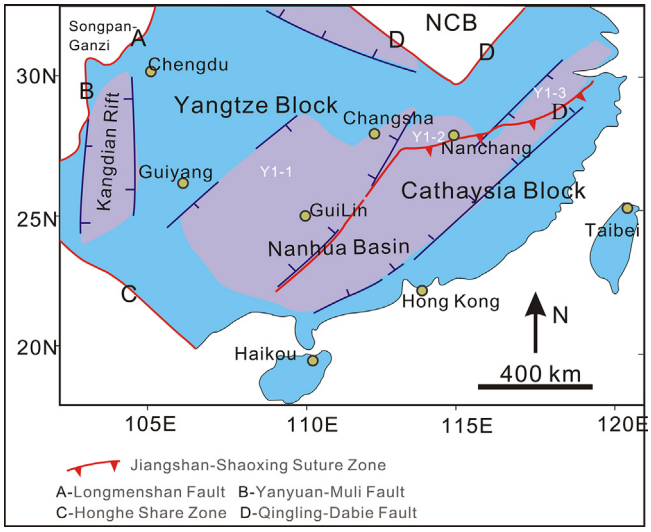

Fig. 1. Schematic map of the Nanhua Basin and other rift basins along the west and north margin of the Yangtze Block (modified from Wang et al., 2014). *Y1-1* Hunan-Guizhou-Guangzi sub-basin, *Y1-2* Jiangnan sub-basin, *Y1-3* Northern Zhejiang sub-basin.

of the basin, the Neoproterozoic and the basal early Cambrian sequence host large manganese, phosphorite, barite, sapropelite, Ni-Mo-*PGE* polymetallic sulfide-rich units and zinc-lead deposits (Fig. 2a).

The Dahebian Zn-Pb deposit is located in the northwestern Nanhua Basin (Tianzhu-Xinhuang-Yuping basin (*TXY* basin); Figs. 1, 2a). There are approximately ten deposits of this type emplaced along the northwestern part of the Nanhua Basin. Some of these deposits, such as Dongjiahe, Dilu, and Laobao have been mined since the 1990s (Luo, 1990; Zeng and Li, 2007; Liang et al., 2009; Liao et al., 2013; Xiang and Luo, 2013; Wen et al., 2017). The Dahebian Zn-Pb deposit is located beneath the vast Dahebian stratiform barite ore deposit, which is considered to have formed through hydrothermal sedimentary exhalative (SEDEX) processes during the early Cambrian (Maynard and Okita, 1991, Xia et al., 2004, 2005; Han et al., 2015). Geological investigation of drill cores from this district showed that the zinc-lead mineralization is primarily discordant but stratabound and is hosted in the Doushantuo Formation (Fig. 3). These sulfide mineralization sites have a close spatial relationship with the stratiform barite ore. However, the genesis of this type of zinc-lead mineralization is not well constrained, especially the relationship between zinc-lead mineralization and stratiform barite mineralization.

In this study, we report data that pertain to the geology, mineralogy, fluid inclusions and S-Pb isotopic compositions of the Dahebian Zn-Pb deposit and the stratiform barite deposit. These data provide insights into the mineralizing fluid and metal source mineralization mechanism, as well as their genetic relationships. This paper also presents a discussion of the possibility of Selwyn-type SEDEX hydrothermal fluid (Cooke et al., 2000) involvement in the ore-forming process, which appears to be critical to the current understanding of hydrothermal events and the change in the paleo-redox seawater condition during the early Cambrian along the Nanhua Basin.

2. Geological settings

The South China Block is generally considered to have been formed through subduction of the Paleo-Huanan oceanic lithosphere beneath both the southeastern margin of the Yangtze Block and the northwestern margin of the Cathaysia Block during the period of 970 Ma–825 Ma and then by collisional amalgamation along the two overriding continental margins at the end of the Jinning Orogeny (ca. 825 Ma–815 Ma) (Li et al., 1999, 2003; Zhao and Cawood, 2012; Zhang et al., 2013). Between ca. 820 Ma and 420 Ma, in the course of breakup of the Rodinia Supercontinent, the South China Block experienced episodic rifting along the Jiangnan Orogen that formed during the Jinning Orogeny (Feng et al., 2010; Zhang et al., 2013), and a southeast-facing passive continental margin on the Yangtze Block was developed throughout rifting. These rifting events were ended by the Guangxi intracontinental orogeny (ca. 540 Ma–405 Ma) (Wang and Li, 2003).

The Nanhua Basin is an intracontinental marine basin that can be traced from Guangxi Province in the west through eastern Guizhou Province, Hunan Province and Jiangxi Province to northern Zhejiang Province (Figs. 1, 2a and 3a). This giant basin was separated by paleo-uplifts, resulting in the formation of numerous sub-basins. From the Neoproterozoic to early Cambrian, the Nanhua Basin consisted of a stratified ocean with oxic shallow water and anoxic deep water (mostly euxinic, ferruginous zones) (Li et al., 2010, 2012; Feng et al., 2010; Wen et al., 2016), as well as hydrothermally induced and accumulated iron, zinc and barium (Lott et al., 1999; Huang et al., 2011; Zhou et al., 2011). The Neoproterozoic to early Cambrian paleogeographic reconstruction reveals a sedimentary zonation from a shallow shelf facies in the northwest to a protected and deep basinal facies in the southeast (Fig. 2; Jiang et al., 2011), which is marked by the upper Ediacaran System and low Cambrian diachronous sequences across the Nanhua Basin.

The basement rock outcrops in the Nanhua Basin were built up by the Lengjiaxi and Banxi Groups and, to a lesser and deeper extent, by crystalline basement rocks. Stratigraphy sequences rest unconformably on the slate rocks of the Banxi Group represent a basinal facies characterized by repeated transgression episodes during rifting in the period ranging from the Neoproterozoic to early Cambrian (Fig. 4). Three types of sedimentary sequences that had been influenced by synsedimentary hydrothermal fluids were distinguished in the basal area of the Niutitang Formation (Fig. 4) including: (1) the sedimentary phosphorite and barite units, (2) sapropelite (combustible shale), up to tens of meters thick, of algal origin, and (3) an organic- and sulfide-rich Ni-Mo-*PGE* ore layer locally distributed in the lower part of the Niutitang Formation with a thickness of a few to two hundred centimeters (Jiang et al., 2006a,b; Wen and Carignan, 2011).

3. Ore geology

3.1. Zn-Pb sulfides mineralization

The Dahebian district consists of a NE-SW-trending fold that formed during the Guangxi intracontinental orogeny (Gongxi syncline, Fig. 3a). The Gongxi syncline is comprises numerous sub-level echelon folds (such as the Benglongshan anticline, Pingdi syncline and Yundong syncline) (Fig. 3a). All of the large barite and sulfide deposits in the Dahebian district are within the Gongxi syncline. The Sangzhi-Jishou-Xinghuang-Tianzhu fault controlled the distribution of the stratiform barite (Fig. 3a; Yang et al., 2008).

The Dahebian Zn-Pb deposit is located in the *TXY* basin (Fang et al., 2002; Wen et al., 2017), which is a continental margin sedimentary basin characterized by the deposition of thick Neoproterozoic to Lower Cambrian sequences of siliciclastic rocks with intercalations of calcareous-shales (Fig. 4). The Doushantuo Formation overlies lower Neoproterozoic slate-siltstone of the Banxi Group and diamictite of the Nanhua System and mainly comprises micrite dolomite and carbonaceous mudstone, with localized phosphorite and chert layers. The Doushantuo Formation is characterized by ulfide ore replacement. The Liuchapo Formation overlies the Doushantuo Formation, and consists of chert with approximately 2 m thick layers of pyritic shale at its center. The Liuchapo Formation, in turn, is overlain by stratigraphically bedded barite deposits or barium-bearing shales from the Lower Cambrian Niutitang Formation. The Jiumenchong Formation conformably overlies the Doushantuo Formation and consists of shale and siltstone.

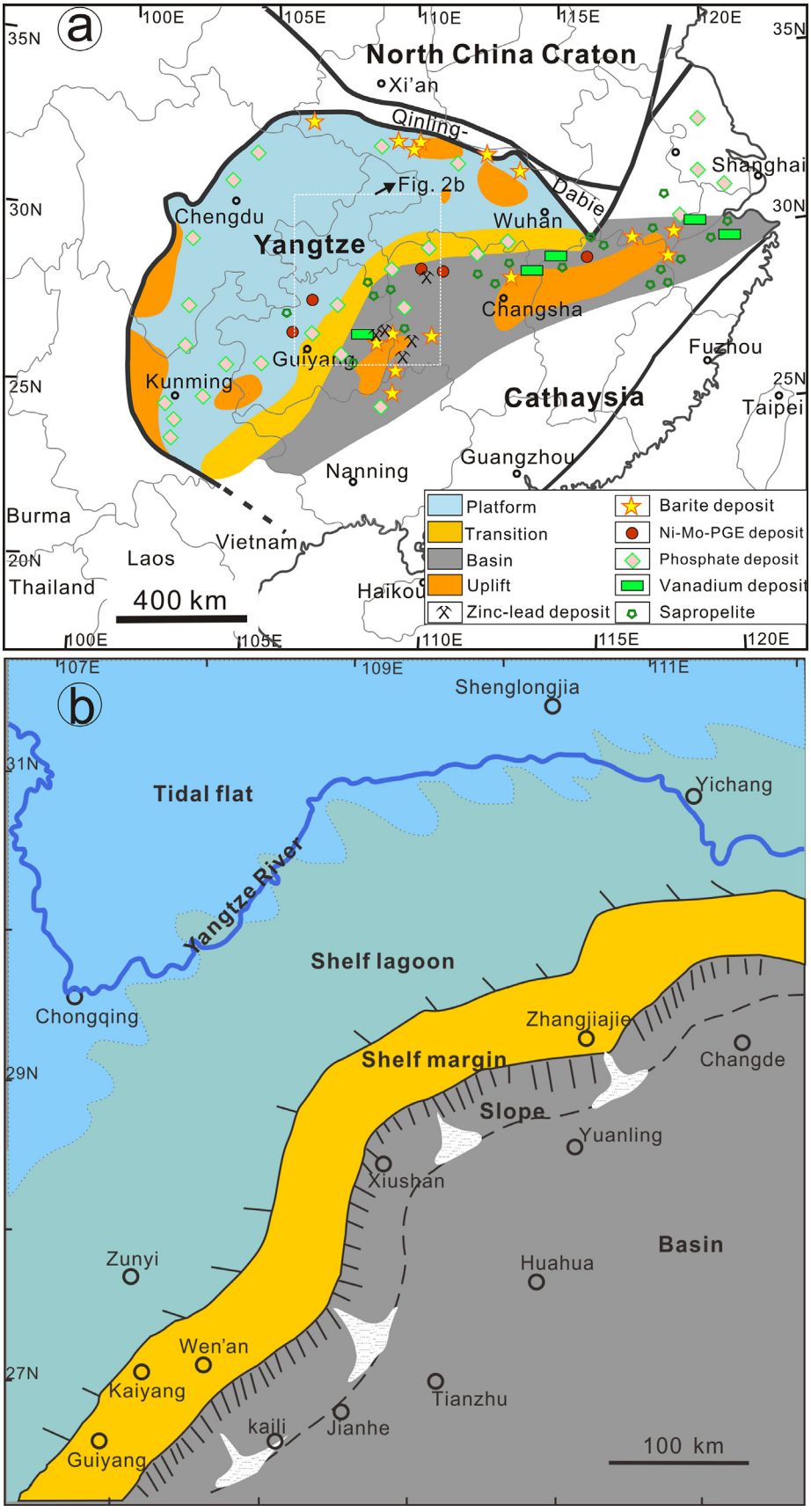

Fig. 2. a. The variety of early Cambrian stratiform ore deposits and the zinc-lead deposit hosted in the Doushantuo Formation on the margin of the Yangtze platform within its early Cambrian geotectonic and paleogeographic setting (modified from Jiang et al., 2011; Lehmann et al., 2016). b. Paleogeographic setting of the Hunan-Guangxi sub-basin during the Ediacaran to Early Cambrian (modified from Jiang et al., 2011) within the location of zinc-lead deposits hosted in the Doushantuo Formation and early Cambrian stratiform barite deposits.

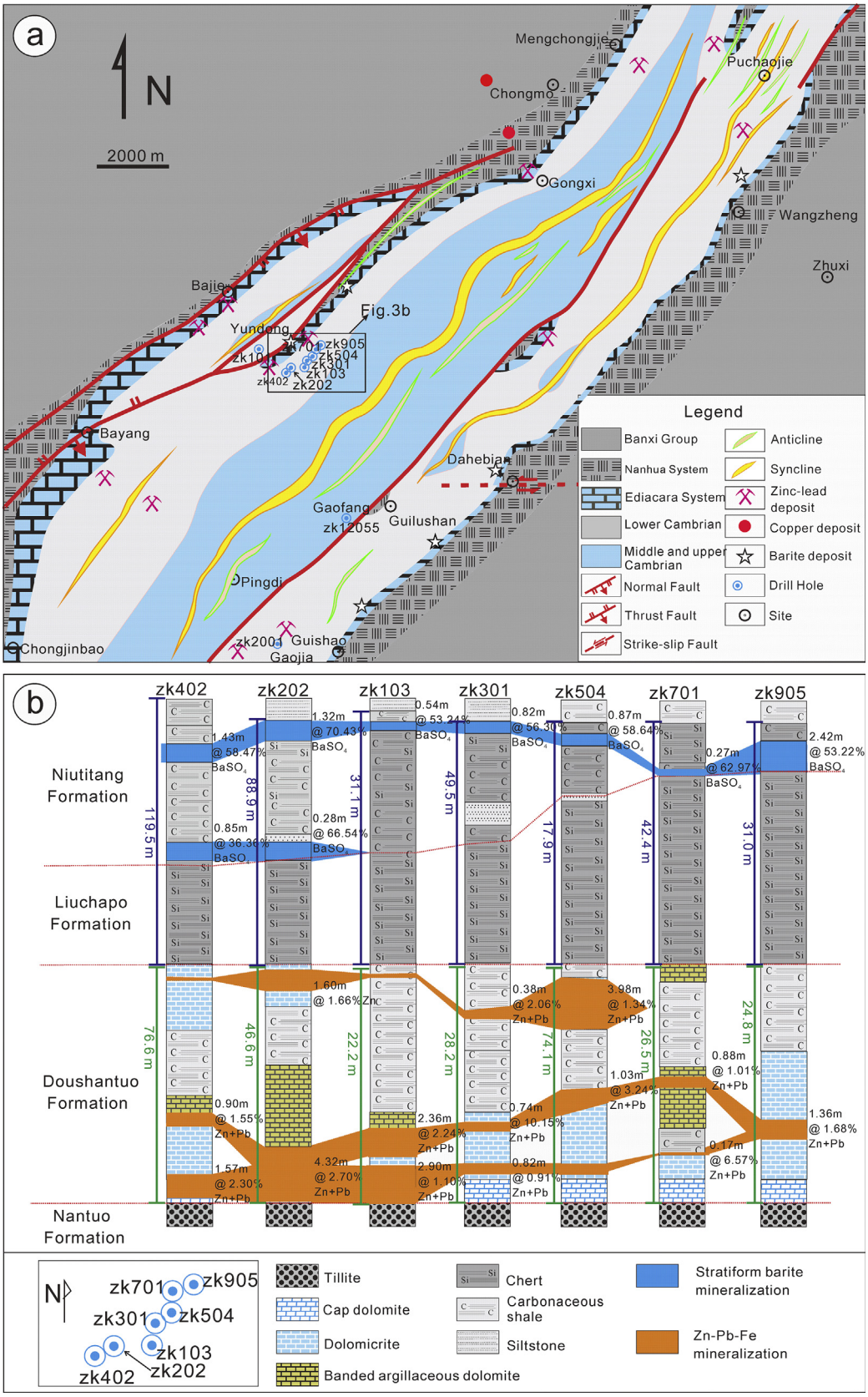

Fig. 3. a. Geological map of the Dahebian district, showing locations of zinc-lead deposits and stratiform barite deposits. b. Correlation diagram of columnar section of drill holes in the Dahebian district.

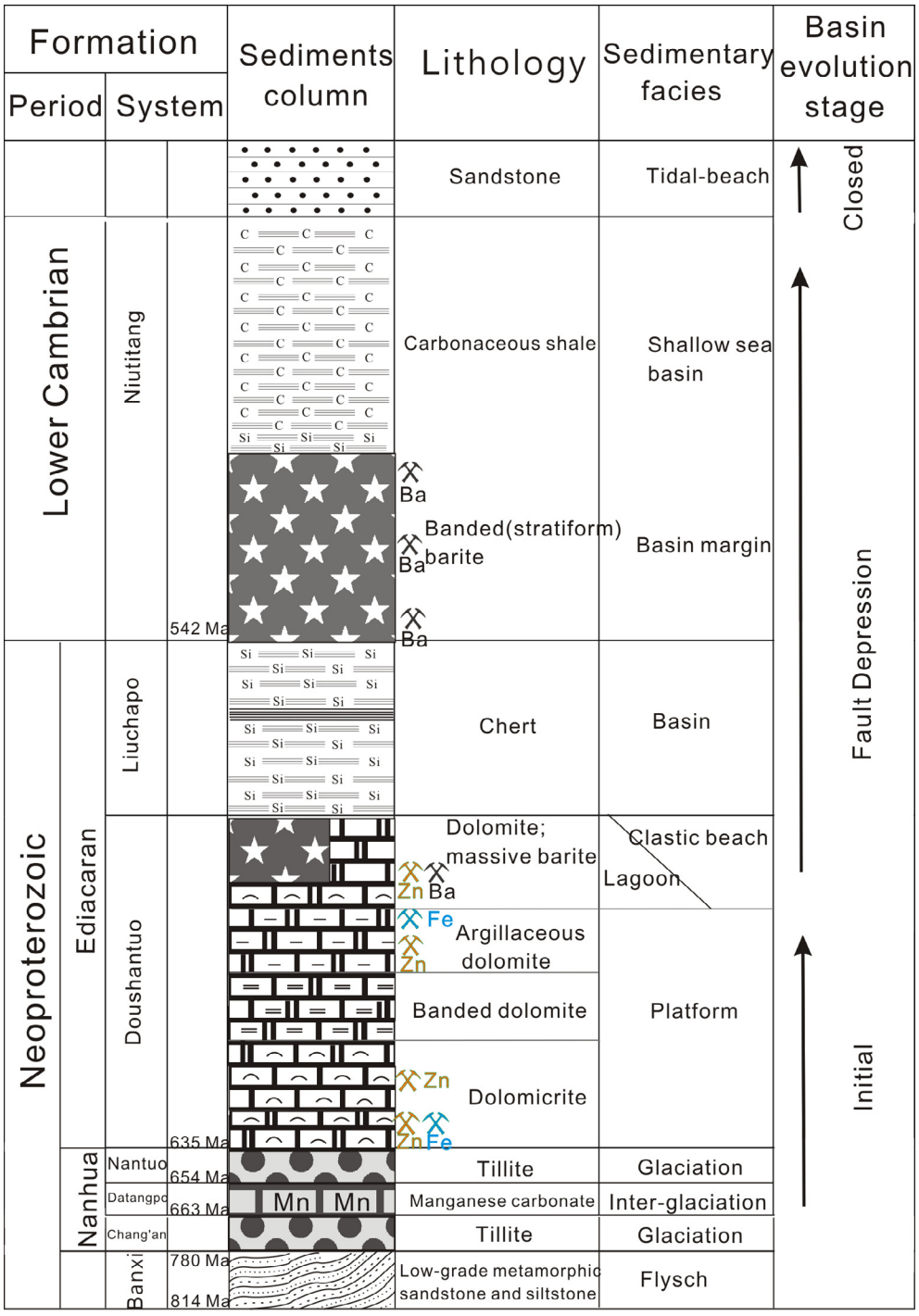

Fig. 4. Stratigraphic section of the Dahebian district, showing locations of zinc-lead sulfide mineralization and stratiform barite mineralization. The crystalline basement mainly consists of the Archean and the Paleoproterozoic metamorphic complexes, which are upper amphibolite-granulite facies metamorphic rocks (Zhai, 2013). The folded basement rocks are represented by Lengjiaxi and Banxi Groups, the former containing mainly greenschist-facies sandstone, siltstone and slate, with minor tuff and mafic-ultramafic dykes (Wang et al., 2004, 2008; Zhao and Cawood, 2012), while the later one consists of low-grade metamorphosed sandstone, siltstone, associated with minor tuff interbeds (Wang et al., 2008; Zhao and Cawood, 2012; Geng, 2015; Zhou et al., 2017). The Lengjiaxi Group is characterized by high-angle upright folds and chevron folds overprint. However, the deformation of Banxi Group appears to be weaker than that of the underlying Lengjiaxi Group. The Banxi Group has a wedge-shaped sequence on a SE-tending section through the Nanhua Basin (Wang et al., 2014), and represents the launch of the rifting event. The Nantuo System which rests unconformably on the slate rocks of the Banxi Group. Two main Nanhua diamictite successions, the lower Chang'an Formation and the upper Nantuo Formation, have been well studied and understood. The interglacial Datangpo Formation of rhodochrosite layers sits on the glacial deposits of the Chang'an Formation (Feng et al., 2010). The Doushantuo Formation overlies the diamictite of the Nantuo Formation and consists of micrite dolomite and carbonaceous mudstone, with localized phosphorite and chert layers. An approximately 30 m-thick chert sequence of the Liuchapo Formation overlies the Doushantuo Formation. The Niutitang Formation of black shales overlies the Liuchapo Formation, which is dominated by black shales and cherts and covered by shale and siltstone of the Jiumenchong Formation.

Based on geological investigations, the mineralization in the Dahebian Zn-Pb deposit has a NE-strike for at least 3.8 km. In an exceedingly narrow area of exploration (approximately 2 km^2), approximately 0.5 Mt grading 0.91–10.15 wt% Zn and 1.24–1.36 wt% Pb have been recorded. Investigations of drill-core samples suggest that the zinc and lead mineralization can be divided into upper and lower layers (Fig. 3b). The lower layer of mineralization is near to the boundary line between the Nantuo Formation and the Doushantuo Formation, primarily hosted in the cap of dolomite. The upper layer of mineralization is hosted in the organic-rich dolomite and shale of the upper part of the Doushantuo Formation (Fig. 3b). Sulfide mineralization in drill cores is usually related to intensive brecciation in the host-rocks, accompanied by silification (Fig. 5c/d/g), and associated with barite, carbonate, and minor organic alteration (Fig. 5). Sphalerite, iron sulfides (such as pyrite and marcasite) and galena are the principal sulfide minerals in the relatively simple mineral assemblage that exists, along with minor amounts of chalcopyrite and stibnite. Quartz and barite are the major gangue minerals, along with negligible amounts of carbonate (dolomite, calcite and witherite), apatite and bitumen of hydrothermal origin. Hyalophane is an accessory mineral and is intergrown with the sulfide minerals.

Sulfide mineralization generally occurs as veins or stock-veins that replaced or filled in the rocks of the Doushantuo Formation (Fig. 5c–g), with minor layers of laminated sulfides (Fig. 5b) and with brecciated textures (Figs. 5e–g, 6a/h). Relatively thick intervals of micrite showing abundant stylolite were filled by sulfides, with small laminated or

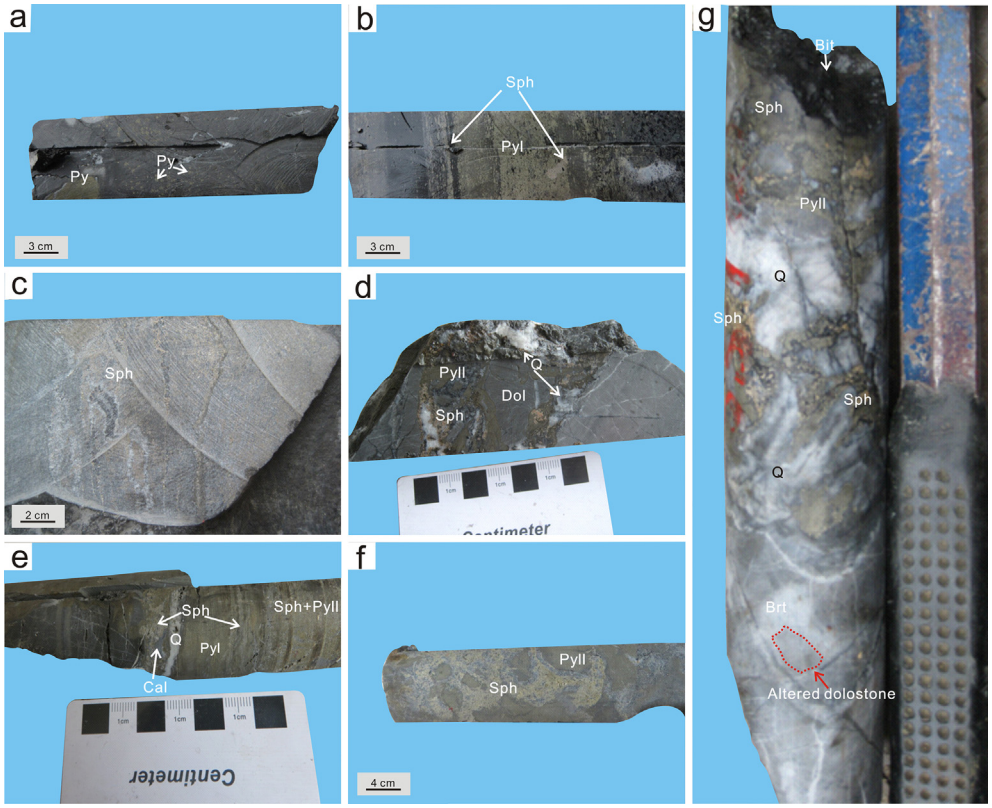

Fig. 5. Examples of sulfide ores in the Dahebian Zn-Pb deposit. a. disperse diagenetic pyrite in carbonaceous siltstone; b. laminated pyrite and sphalerite; c. fine grained sphalerite disseminated in dolostone; d. fine grained pyrite intergrowth with pale-yellow sphalerite and replacing host rock; e. fine grained sphalerite filling interspaces between early stage course grained pyrite; f. pale-yellow sphalerite replacing fine grained pyrite; g. sphalerite and fine grained pyrite distributed in quartz veins and the intense silicification through dolostone. Abbreviations: *Py*-Pyrite; *Sph*-Sphalerite; *Brt*-Barite; *Cal*-Calcite; *Q*-Quartz; *Bit*- Bitumen. (For interpretation of the references to colour in this figure legend, the reader is referred to the web version of this article.)

disseminated textures (Fig. 5c). To a lesser extent, some drill-cores show a laminated fine-grained sphalerite and pyrite layer at the base of the Niutitang Formation. The laminated fine-grained sphalerite and pyrite layers are laterally semi-continuous units. Hydrothermal stage pyrite in the ore is usually coarse-cubic grained (Figs. 5a/b, 6a/d) or fine grained (Fig. 5e/f, 6a/b/f).

Based on the extensive textural and mineralogical associations observed in the drill core samples, the mineralization process can be classified into four stages (Fig. 8) as follows: (1) the diagenetic stage, and (2–4) hydrothermal stages I, II and III. In the diagenetic stage, framboidal pyrite is randomly distributed in the organic-rich micrite and shale of the Doushantuo Formation (Fig. 5a). Minor amounts of barite and apatite were recrystallized when the Doushantuo Formation entered the diagenetic stage (Shields et al., 1999; Zhou et al., 2010; Huang et al., 2011). Hydrothermal stage I contains massive coarse-cubic pyrite co-precipitated with red-brown sphalerite, quartz and bitumen, along with minor amounts of apatite and hyalophane. This stage is predominantly accompanied with brecciation with silification to the host-rock. Hydrothermal stage II is represented by fine-grained pyrite, acicular marcasite and pale-yellow sphalerite co-precipitated with quartz and barite, minor amounts of galena, hyalophane (Fig. 6h, i), dolomite and anhydrite. Finally, in hydrothermal stage III, barite occurs in association with minor amounts of pyrite, sphalerite, galena, chalcopyrite, witherite and dolomite that precipitated as fission veins and cross-cuts in earlier generations of mineralization.

3.2. The stratiform barite mineralization

The Dahebian stratiform barite deposit is situated mainly in the basal layer of the Niutitang Formation. The stratiform barite ore horizon overlies chert of the Liuchapo Formation and is covered by black shale and siltstone (Wang et al., 1991).

This deposit has a NE-strike on a length of at least 20 km, and containing more than 250 Mt of ore grading 85.6 wt% $BaSO_4$ (Tian et al., 2014). Moreover, the barite ore is remarkable as it is enriched in zinc, mostly with concentrations above 0.6 wt% (with a mean of 0.65 wt%). The ore-horizon generally has a thickness of 1–5 m, with a maximum of 10.2 m. The principal ore mineral is barite, accompanied with chert, hyalophane and apatite, minor amounts of carbonate (dolomite and witherite) and sulfide minerals (sphalerite, chalcopyrite, pyrite, stibnite and galena).

4. Samples and methods

4.1. Sampling

Over 600 Samples were collected from 7 recent drill-cores from the Dahebian district (Fig. 3). Each drill core was sampled systematically at 1-m intervals. Polished petrographic and fluid inclusion sections were prepared to provide a representative suite of samples. On the basis of detailed work on the petrography and fluid inclusions, we chose representive samples to crush using a 40–80 mesh. We then handpicked selected sulfides and sulfates using a stereoscopic microscope. Sufficient quantities of whole rock samples, sulfides and sulfates were crushed using an agate mortar before using a 200 mesh.

4.2. Methods

Fluid inclusion petrography, microthermometric measurements and petrographic analysis was carried out at the State Key Laboratory of Ore Deposit Geochemistry (SKLODG), Institute of Geochemistry, Chinese Academy of Sciences, Guiyang in Guizhou Province. Microthermometric data of fluid inclusions were based on the observations of phase transitions of fluid inclusions at −196 to 600 °C in quartz, barite and sphalerite using a *Linkam THMSG-600* heating-freezing stage, coupled with a Zeiss microscope. Freezing runs were done with a precision of ± 0.1 °C for ice melting; heating runs were done with a precision is ± 0.5 °C for the critical point. Salinity expressed as weight percent NaCl eq. (wt% NaCl eq.) was calculated from microthermometric data, using the equations provided by Bodnar (1993).

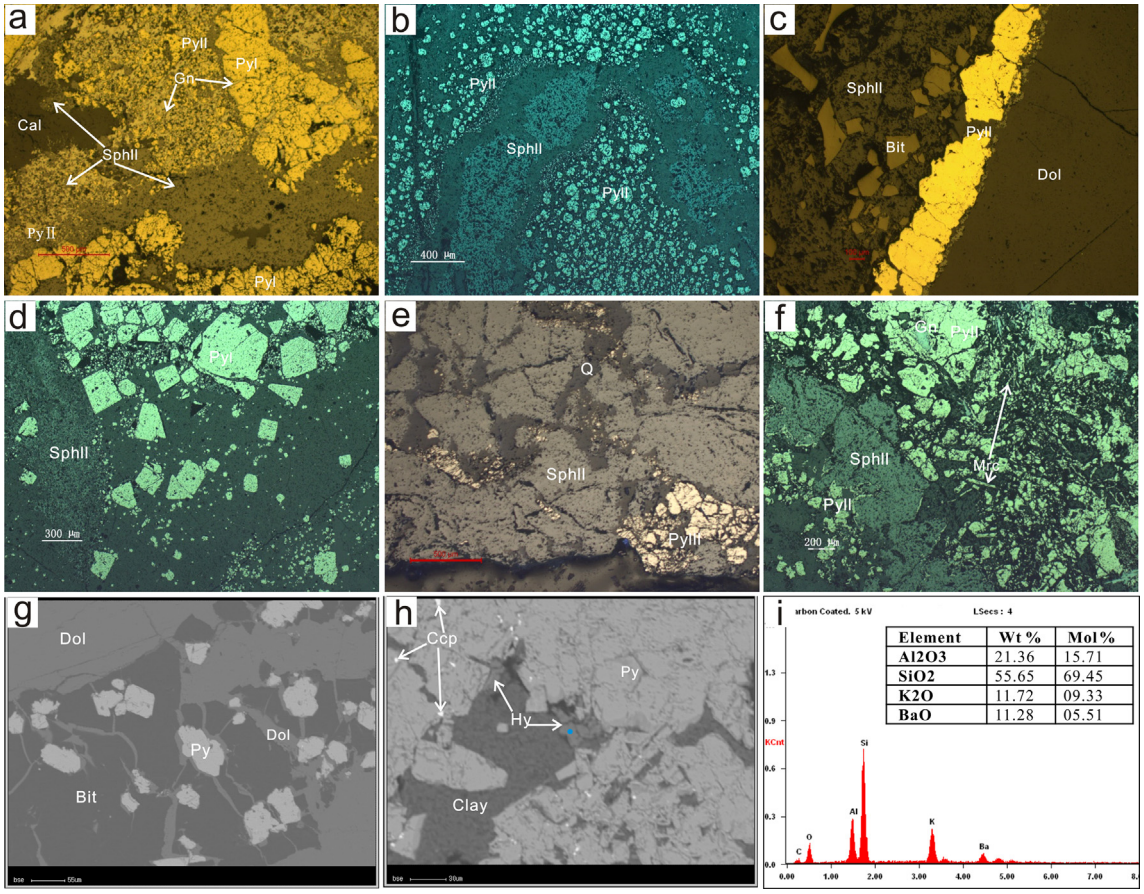

Fig. 6. Photomicrography of samples collected from the Dahebian Zn-Pb deposit. a. sphalerite, fine grained pyrite and pyrite fill into the void between earlier stage coarse grained pyrite; b. sphalerite intergrowth with fined grained pyrite; c. pyrite and sphalerite intergrowth with bitumen and crystallized around dolostone; d. late stage coarse-grained pyrite; e. late stage pyrite and quartz replacing sphalerite; f. pyrite and marcasite intergrowth with sphalerite, pyrite layer around sphalerite as the corona texture; g. pyrite grains in the bitumen, these pyrite grains always coated with dolomite; h. hyalophane grains around pyrite; i. the EDS image showing the composition of hyalophane grain marked by blue point in Fig. 5-h. Photomicrograph a–f were taken under reflected light, g-h were taken with a backscattered electron microscope. Assbbreviations: *Q*-Quartz; *Sph*-Sphalerite; *Gn*-Galena; *Ccp*-Chalcopyrite; *Py*-Pyrite; *Mr*-Marcasite; *Dol*-Dolomite; *Cal*-Calcite; *Bit*-Bitumen; *Hy*-Hyalophane.

Scanning electron microscope analyses were done on a Japan Electron Optics Limited (JEOL) JSM-7800F Superprobe® equipped with energy dispersive spectrometers (EDS) at the SKLODG. EDS spot analyses were done using a beam diameter of 1 μm, a beam current of 50nA, an accelerating potential of 20 kV, a dwell time of 30 s on peak, and a 30-s off-peak background on either side of the peak.

Sulfide minerals (including sphalerite and pyrite) and barite were prepared for sulfur isotopic analysis. The analysis was carried out using a Flash-EA-MAT-253 mass spectrometer at the SKLODG. The sulfide minerals and the mixture of barite-V_2O_5 were combusted with copper oxide in a vacuum at 1000 °C to produce SO_2 gas for analysis by isotopic ratio-monitoring (Robinson and Kusakabe, 1975). Isotopic data were reported as $\delta^{34}S$ values relative to VCDT of IAEA-S-1 ($\delta^{34}S_{VCDT} = -0.30‰$), IAEA-S-2 ($\delta^{34}S_{VCDT} = 22.62‰$) and IAEA-S-3 ($\delta^{34}S_{VCDT} = -32.49‰$). The relative error at 2σ was better than 0.1‰.

Sulfide samples (sphalerite, galena and pyrite) and representative sedimentary rock samples were selected to measure lead isotopic compositions. These measurements were performed at the SKLODG, using a *Thermo-Scientific Neptune plus* MC-ICP-MS coupled with a membrane desolvation system (*CETAC Aridus II*). Lead was separated and purified by using a conventional cation-exchange technique, with diluted HBr as the eluant. Lead isotopes are reported relative to the measured ratio of NBS 981 ($^{206}Pb/^{204}Pb = 16.9327 \pm 0.0002$, $^{207}Pb/^{204}Pb = 15.4843 \pm 0.0004$, and $^{208}Pb/^{204}Pb = 36.6856 \pm 0.0001$) and corrected for instrument mass fractionation. The precision of $^{208}Pb/^{206}Pb$ measurements (1 μg of Pb) is better than 0.001%.

5. Results

5.1. Petrography

The results of ore microscopy observations are summarized in Figs. 5–7. Hyalophane in the stratiform barite ore and the shale in the middle of the Liuchapo Formation is mostly xenomorphic and granular, intergrown with barite, pyrite, apatite and fine-grained sphalerite. Some pyrite inlaid in hyalophane display mosaic and/or zoned structures (Fig. 7c, d). However, compared to its abundant appearance in the stratiform barite ore, hyalophane is rare in theZn-Pb sulfide ores. There hyalophane occurs as small particles with a diameter of 10–200 μm, in a co-precipitation with sphalerite, pyrite and apatite. We selected typical hyalophane for EDS analyses, to better understand the ore mineralogy as well as the physicochemical conditions of the zinc-lead mineralization and the barite mineralization. The analytical results are presented in Table 1.

Hyalophane has a theoretical formula of (K, Ba) $Al_2Si_2O_8$. Hyalophane in the stratiform barite contains SiO_2 concentrations of 45.26–52.58% (mean = 48.81%; n = 8), Al_2O_3 concentrations of 20.38–24.16% (mean = 23.27%; n = 8), K_2O concentrations of 4.68–6.52% (mean = 5.52%; n = 8), BaO concentrations of 18.36–25.89% (mean = 21.12%, n = 8), the sample of hyalophane tznp-62 contain As_2O_3 concentrations of 1.44%. Hyalophane in shale situated at the middle of the Liuchapo Formation contains SiO_2 concentrations of 62.21–69.62% (mean = 67.15%; n = 3), Al_2O_3

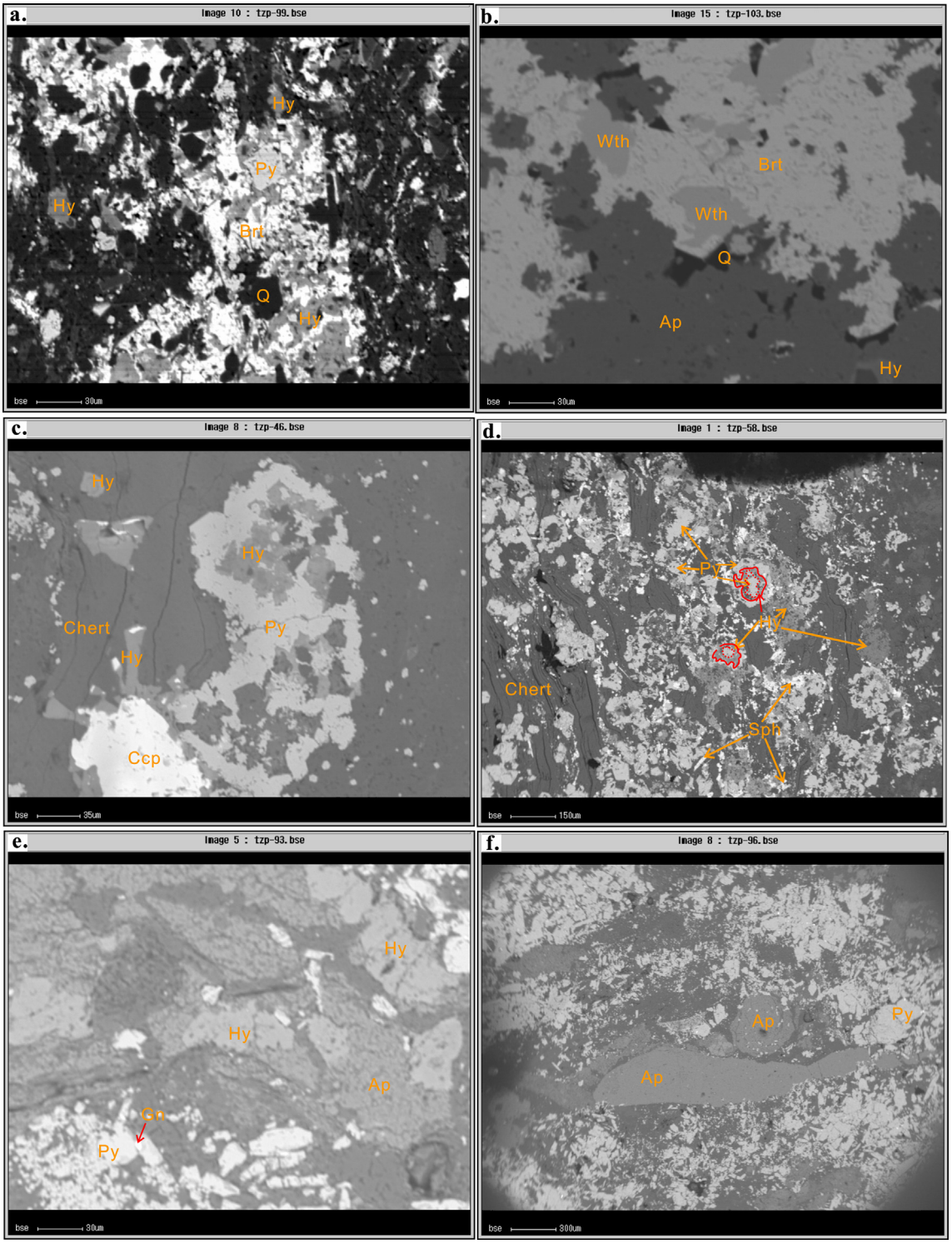

Fig. 7. Backscattered electron (BSE) photomicrographys of ores selected from the Dahebian Zn-Pb deposit and stratiform barite deposit. a. hyalophane intergrowth with barite and minor pyrite; b. barite and witherite intergrowth with apatite; c. hyalophane encircled with pyrite, hyalophane also scattered around chalcopyrite, both of them were parallel with micro-layers of chert; d. zonal growth of pyrite and hyalophane, there also exist minor amounts of acicular sphalerite; e. pyrite and galena, fill into the interspace between apatite and hyalophane grains; f. apatite nodules among fine grained pyrite. a–d were taken from the stratiform barite deposit and e-f were taken from the Pb-Zn deposit. Abbreviation: *Hy*- Hyalophane; *Wth*-Witherite; *Sph*-Sphalerite; *Gn*-Galena; *Ccp*-Chalcopyrite; *Py*-Pyrite.

concentrations of 15.65–19.71% (mean = 17.00%; n = 3), K_2O concentrations of 4.50–9.44% (mean = 6.15%; n = 3), BaO concentrations of 8.65–10.23% (mean = 9.70%, n = 3). Hyalophane in the Zn-Pb sulfide ores contain SiO_2 concentrations of 47.76–55.65% (mean = 51.46%; n = 6), Al_2O_3 concentrations of 20.42–23.18% (mean = 21.84%; n = 6), K_2O concentrations of 7.44–11.72% (mean = 9.23%; n = 6), BaO concentrations of 11.28–19.87% (mean = 16.58%, n = 6), samples of hyalophane tznp-62 and tznp-63 have P_2O_5 concentrations of 2.00% and CaO concentrations of 3.41%, respectively.

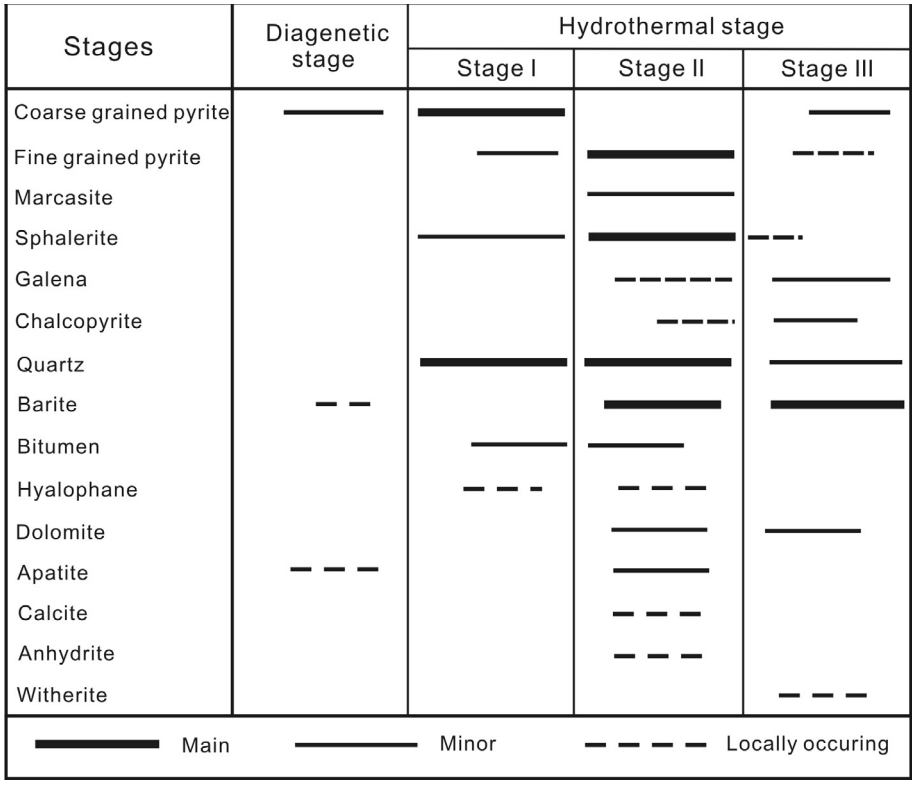

Fig. 8. Simplified paragenetic sequence of ore and gangue minerals from the Dahebian Zn-Pb deposits.

5.2. Fluid inclusions

Fluid inclusions trapped in sphalerite commonly vary in size from 5 to 15 μm, with minor amounts exceeding 20 μm in size. These fluid inclusions have two phases (liquid + vapor) with a vapor phase ranging from 10 to 20 vol% of the whole inclusion (Fig. 9). They always have negative crystal distribution and an oval shape. Upon freezing these inclusions formed a brown, granular ice at about −81 to −90 °C (mean = −87 °C). The first melting of ice was observed at −52 to −56 °C (mean = −54 °C). The final melting of ice occurred between −24.4 and −0.6 °C, corresponding to salinities of 1.05–25.62 wt% NaCl eq. (Table 2, Appendix A). Inclusions are homogenized into a liquid phase between 142 and 317 °C.

Based on the phases and estimated volumetric proportion of vapor to liquid present at room temperature, fluid inclusions trapped in sulfidic mineralization stage quartz can be divided into two types. Type I inclusions are characterized by a dominant aqueous fluid and are rare in all examined samples. Type II inclusions have two phases (liquid + vapor), the vapor phase typically occupies 10–30 vol% of the total inclusion, and are oval in shape with some having an irregular shape. Type II inclusions mostly vary in size from 5 to 20 μm, a few fluid inclusions exceeding 30 μm in size. Upon freezing these inclusions formed a brown, granular ice at about −63 to −59 °C (mean = −61 °C). The first melting of ice was observed at about −30 °C. Last ice melting occurred between −7.6 and −0.3 °C, corresponding to salinities of 0.53–11.23 wt% NaCl eq. Inclusions are homogenized into a liquid phase between 165 and 368 °C.

Fluid inclusions confined in barite can be divided into two types, based on the volumetric proportion of the vapor phase to liquid present at room temperature. Type II inclusions have two phases

Table 1
Compositions of hyalophane within the Dahebian Zn-Pb deposit, the middle of the Liuchapo Formation and stratiform barite deposit, determined by EDS (wt%).

Samples location	Spot No.	Al_2O_3	SiO_2	K_2O	BaO	P_2O_5	CaO	As_2O_3	Molecular formula
Stratiform barite deposit	tznp-57	20.38	46.95	4.70	19.17				$K_{0.34}Ba_{0.86}Al_{1.37}Si_{2.67}O_8$
	tznp-58	22.96	52.58	6.10	18.36				$K_{0.40}Ba_{0.73}Al_{1.38}Si_{2.68}O_8$
	tznp-61	23.80	51.18	6.42	18.61				$K_{0.42}Ba_{0.75}Al_{1.44}Si_{2.63}O_8$
	tznp-62	23.46	50.86	6.18	19.51			1.44	$K_{0.41}Ba_{0.79}Al_{1.43}Si_{2.63}O_8$
	tznp-63	24.09	48.19	5.34	20.94				$K_{0.36}Ba_{0.87}Al_{1.51}Si_{2.56}O_8$
	tznp-147	23.70	46.05	4.99	25.26				$K_{0.35}Ba_{1.08}Al_{1.52}Si_{2.50}O_8$
	tznp-164	24.16	45.26	4.68	25.89				$K_{0.33}Ba_{1.11}Al_{1.56}Si_{2.47}O_8$
	tznp-166	23.61	49.4	5.79	21.20				$K_{0.39}Ba_{0.87}Al_{1.46}Si_{2.59}O_8$
The middle of the Liuchapo Formation	tznp-115	15.65	69.62	4.50	10.23				$K_{0.26}Ba_{0.37}Al_{0.85}Si_{3.20}O_8$
	tznp-116	15.65	69.62	4.50	10.23				$K_{0.26}Ba_{0.37}Al_{0.85}Si_{3.20}O_8$
	tznp-117	19.71	62.21	9.44	8.65				$K_{0.57}Ba_{0.32}Al_{1.10}Si_{2.95}O_8$
	tznp-123	22.46	47.76	7.92	19.87	2.00			$K_{0.55}Ba_{0.84}Al_{1.43}Si_{2.58}O_8$
	tznp-125	23.18	50.42	9.06	17.35				$K_{0.60}Ba_{0.70}Al_{1.42}Si_{2.61}O_8$
Zinc-lead deposit	tznp-128	21.36	55.65	11.72	11.28				$K_{0.74}Ba_{0.44}Al_{1.25}Si_{2.77}O_8$
	tznp-130	21.53	48.56	8.97	17.54		3.41		$K_{0.60}Ba_{0.73}Ca_{0.19}Al_{1.34}Si_{2.57}O_8$
	tznp-133	22.07	51.48	10.29	16.16				$K_{0.68}Ba_{0.65}Al_{1.34}Si_{2.66}O_8$
	tznp-137	20.42	54.86	7.44	17.28				$K_{0.48}Ba_{0.69}Al_{1.22}Si_{2.79}O_8$

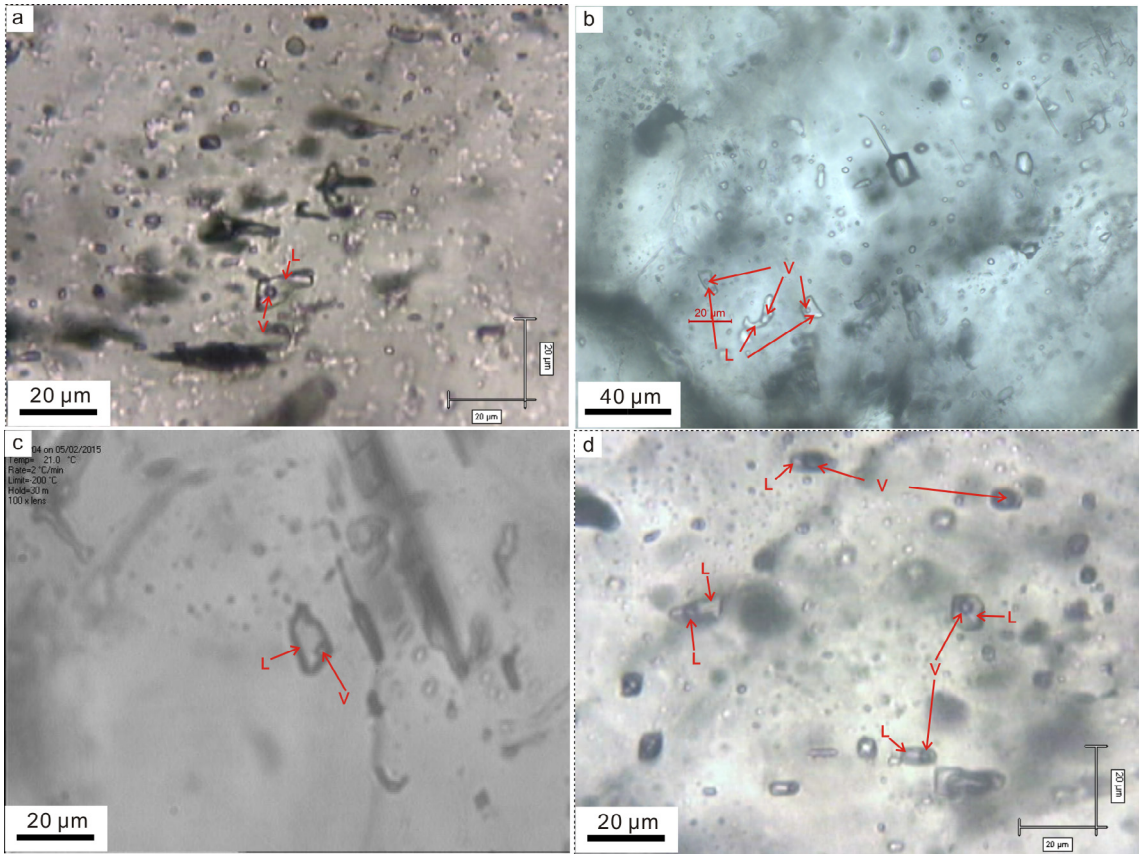

Fig. 9. Photomicrographs of fluid inclusions in the Dahebian Zn-Pb deposit.

Table 2
Summary of aqueous fluid inclusion data for the Dahebian deposit.

Mineral	Sample No.	Number	Tm/clath-ice (°C)	Th (°C)	Salinity (wt% NaCleq.)
Sphalerite	Zk902-2	21	−24.4 to −1.2 (−9.9)	142–255 (190)	2.06–25.62 (11.60)
	03H22	3	−2.3 to −1.3 (−2.0)	188–317 (252)	2.23–9.85 (3.31)
	Zk202H75	4	−1.5 to −0.6 (−1.1)	195–317 (262)	1.04–2.56 (1.93)
Quartz	Zk902-2	21	−7.6 to −1.5 (−3.4)	165–353 (256)	2.56–11.23 (5.45)
	Zk202H77	6	−1.2 to −0.4 (−0.8)	222–368 (284)	1.89–7.81 (1.30)
	Zk202H75	9	−1.4 to −0.3 (−0.8)	177–320 (253)	0.53–2.40 (1.31)
Barite	Zk902-1	24	−11.4 to −1.5 (−5.8)	142–198 (170)	2.56–15.45 (8.59)
	Zk202H77	13	−2.6 to −0.3 (−1.3)	158–308 (208)	0.52–4.32 (2.14)
	Zk202H75	4	−0.8 to −0.3 (−0.5)	228–320 (279)	0.53–1.40 (0.93)

Note: Partly data were cited from Wen et al. (2017).

(liquid + vapor) with the vapor phase ranging from 10 to 20 vol% of the whole inclusion. These inclusions are elongate to rounded in shape with a few having an irregular form. Type III inclusions have two phases (liquid + vapor) with the vapor phase beyond 40 vol% of the whole inclusion. The observed shapes have an orthogonal, hexagonal and elongated morphology. Upon freezing, these inclusions formed a brown, granular ice at about −60 to −50 °C (mean = −56 °C). The first melting of ice was observed between approximately −40 to-28 °C. The final melting of the ice occurred between −11.4 and −0.3 °C, corresponding to salinities of 0.53–15.45 wt% NaCl eq. The inclusions homogenized into a liquid phase between 142 and 320 °C.

5.3. Sulfur isotopic compositions

The $\delta^{34}S_{VCDT}$ values of sulfides (sphalerite and pyrite), barite selected from Zn-Pb sulfides and stratiform barite ore are listed in Table 3 and shown in Fig. 11. The $\delta^{34}S_{VCDT}$ values of sulfide samples range from 13.5‰ to 30.0‰ with an average value of 20.5 ± 3.1‰ (n = 30). These samples record a relatively narrow range of $\delta^{34}S_{VCDT}$ values, *i.e.*, 13.5‰–22.9‰ (n = 15, mean = 19.6 ± 2.9‰) for sphalerite and 15.0‰–30.0‰ (n = 15, mean = 21.4 ± 3.2‰) for pyrite. The ranges of $\delta^{34}S_{VCDT}$ values of barite selected from Zn-Pb sulfide ores range from 29.5‰ to 57.4‰ (n = 4, mean = 40.0 ± 12.1‰), and the samples selected from the stratiform barite ore have values ranging from 29.5‰ to 55.1‰ (n = 45, mean = 40.4 ± 4.3‰).

5.4. Lead isotopes

Lead isotopic compositions of sulfides, barite and host rocks from the Zn-Pb sulfides and the stratiform barite ore, together with those of

Table 3
Sulfur isotope of sulfide minerals and barite from the Dahebian Zn-Pb deposit and stratiform barite deposit.

Sample No.	Depth (m)	Mineral	$\delta^{34}S_{VCDT}$ (‰)	Sample No.	Depth (m)	Mineral	$\delta^{34}S_{VCDT}$ (‰)
GS-2	–	Barite	39.39	zk202H121	204.5	Pyrite	25.31
GS-3	–	Barite	39.01	zk202H121	204.5	Sphalerite	19.23
DHB-1	–	Barite	42.43	zk202H123-125	206.0	Sphalerite	18.39
zk202H2	54.0	Barite	32.26	zk202H127	209.8	Pyrite	25.44
zk202H10	63.6	Barite	48.31	zk202H127	209.8	Sphalerite (Red-brown)	14.28
zk202H37	98.5	Pyrite	29.96	zk001	–	Sphalerite (Red-brown)	13.49
zk202H48	113.5	Pyrite	17.52	zk001-3	–	Sphalerite (Pale-yellow)	22.89
zk202H75	154.3	Barite	57.41	zk501H69-H72	–	Sphalerite (Pale-yellow)	18.36
zk202H75-1	154.3	Pyrite	22.39	zk701H36-37	–	Sphalerite (Pale-yellow)	18.19
zk202H83	161.6	Fine-grained pyrite	19.15	zk902-1	–	Sphalerite (Pale-yellow)	21.11
zk202H83-1	161.6	Coarse-grained pyrite	19.25	zk902-2	–	Sphalerite (Pale-yellow)	21.65
zk202H87	165.6	Fine-grained pyrite	21.07	zk902-3	–	Sphalerite	21.64
zk202H87-1	165.6	Coarse-grained pyrite	20.15	zk902-4-1	–	Sphalerite (Red-brown)	22.56
zk202H97	174.6	Fine-grained pyrite	21.15	zk902-4-2	–	Sphalerite (Pale-yellow)	21.30
zk202H97-1	174.6	Coarse-grained pyrite	20.26	zk902-4-1-1	–	Sphalerite (Pale-yellow)	21.54
zk202H103	181.3	Sphalerite	21.55	zk902-1	–	Barite	29.51
zk202H111	192.0	Fine-grained pyrite	19.36	zk902-1	–	Barite	36.00
zk202H111-1	192.0	Coarse-grained pyrite	19.64	zk902-1	–	Barite	37.08
zk202H117	200.8	Pyrite	20.75	zk902-2	–	Barite	36.33
zk202H117	200.8	Sphalerite	17.87				

the basement rocks and Mississippi valley type (MVT) zinc-lead deposits adjacent to the Dahebian district, are summarized in Table 4 and shown in Fig. 12 (full data are shown in Appendix B).

Sulfides representing the Zn-Pb sulfide mineralization have a range of $^{206}Pb/^{204}Pb$ rations from 17.6790 to 17.7177 (mean = 17.6940), $^{207}Pb/^{204}Pb$ from 15.5370 to 15.5773 (mean = 15.5683), and $^{208}Pb/^{204}Pb$ from 37.5870 to 37.7159 (mean = 37.6873). The lead isotopic data of the sulfides selected from the stratiform barite ore show a slightly radiogenic, which have a range of $^{206}Pb/^{204}Pb$, $^{207}Pb/^{204}Pb$ and $^{208}Pb/^{204}Pb$ rations range from 17.9707 to 18.8165 (mean = 18.4252), 15.6743–15.7212 (mean = 15.6961) and, 38.0255–38.6187 (mean = 38.2638), respectively.

U and Th content of sedimentary rocks are relatively high and may influence their lead isotopic compositions. Hence, lead isotopic compositions of these sedimentary rocks need to be corrected with age (*e.g.*, Carr et al., 1995; Muchez et al., 2005). The Ni-Mo-*PGE* polymetallic sulfide-rich units, overlies on the stratiform barites ores, with formed age of 541 ± 16 Ma (molybdenum-nickel ore samples Re-Os isochron age, Mao et al., 2002). Besides, the stratiform barite ores located at the basal Cambrian system. So 542 Ma was used to correct the lead isotope. After correction, the host rock of Zn-Pb sulfide mineralization have a range of $^{206}Pb/^{204}Pb$ ratios from 17.7270 to 19.3290 (mean = 18.1940), $^{207}Pb/^{204}Pb$ from 15.5750 to 15.6670 (mean = 15.6140), and $^{208}Pb/^{204}Pb$ from 37.6860 to 38.0440 (mean = 37.8490); the stratiform barite ore and interbedded shale have a range of $^{206}Pb/^{204}Pb$ rations from 16.3453 to 18.7599 (mean = 17.8015), $^{207}Pb/^{204}Pb$ from 15.4855 to 15.7065 (mean = 15.6415), and $^{208}Pb/^{204}Pb$ from 37.3690 to 38.3430 (mean = 37.9559).

6. Discussion

6.1. The linkage between Zn-Pb sulfide mineralization and stratiform barite mineralization

Zn-Pb sulfide mineralization and stratiform barite mineralization have a close spatial relationship. Gaps between sulfide mineralization and stratiform barite mineralization consist of chert and shale of the Liuchapo Formation, mostly less than 30-m thick (Fig. 3b). The sulfides and stratiform barite ore have similar mineralization element associations. Barium concentrations in Zn-Pb sulfide ores are notably high, with a range of 1230–16,600 ppm (mean = 6193 ppm, zk 202). Zinc shows a remarkable enrichment in the stratiform barite deposit, with a range from 334 ppm to 7220 ppm (mean = 2598 ppm, zk 202). Abundant barite is present in the sulfide ores and shows an intergrowth relationship with the sulfide minerals. In the Xinhuang region (the northeastern Dahebian district), an approximately 5-m thick layer of barite on the upper part of the sulfide mineralization was exploited for

Table 4
Summary of Pb isotopic composition of sulfides, barite and sedimentary rocks in the Dahebian district.

Sample Type	Number of Samples	$^{208}Pb/^{204}Pb$	$^{207}Pb/^{204}Pb$	$^{206}Pb/^{204}Pb$	μ value
Dahebian zinc-lead deposit					
Pyrite	6	37.6966–37.7134 (37.7052)	15.5721–15.5762 (15.5739)	17.6853–17.7033 (17.6918)	9.62–9.69 (9.65)
Sphalerite	20	37.5870–37.8010 (37.7198)	15.5370–15.5863 (15.5741)	17.5971–17.7499 (17.7035)	9.43–9.52 (9.50)
Dahebian strariform barite deposit					
Galena	4	38.0255–38.6187 (38.2638)	15.6961–15.6743 (15.6961)	17.9707–18.8165 (18.4252)	9.62–9.69 (9.65)
Barite and shales	15	37.3690–38.1903 (37.8902)	15.4855–15.7065 (15.6253)	16.3453–18.7599 (17.7522)	9.59–16.13 (10.53)
MVT zinc-lead deposit					
Huayuan	51	38.099–38.888 (38.373)	15.524–15.875 (15.721)	18.028–18.293 (18.173)	9.33–10.03 (9.73)
Basement					
Banxi Group	25	37.897–41.640 (39.031)	15.430–15.705 (15.542)	15.528–20.106 (18.004)	9.24–10.01 (9.43)
Lengjiaxi Group	7	39.294–46.917 (41.870)	15.586–15.937 (15.715)	18.832–22.038 (19.993)	9.39–11.25 (9.82)
Sedimentary rocks					
Doushantuo Formation	7	37.686–38.044 (37.849)	15.575–15.667 (15.614)	17.727–19.329 (18.194)	9.49–9.93 (9.59)
Liuchapo Formation	4	37.919–38.343 (38.137)	15.636–15.686 (15.659)	17.559–18.484 (17.937)	10.57–18.35 (13.83)
Qingxudong Formation	12	38.107–39.408 (38.483)	15.479–15.783 (15.665)	17.204–19.073 (18.285)	9.35–9.79 (9.61)

several years. In the stratiform barite ore, we observed abundant of fine-grained pyrite, chalcopyrite and sphalerite minerals intergrown with barite, as well as a few samples at the bottom of the stratiform barite sequence displaying fine-grained laminated sphalerite/pyrite layers.

In addition to both the principal sulfide and sulfate minerals that can be found in sulfide and/or sulfate ores, the accessory mineral hyalophane is present both in the sulfides and the stratiform barite ore. Hyalophane has the ideal formula (K, Ba) $Al_2Si_2O_8$ and forms in the binary solid-solution series between potassium and barium feldspars. Hyalophane is typically associated with exhalative hydrothermal processes and low to medium grade metamorphism (Jakobsen, 1990; Fortey et al., 1993; McSwiggen, 1994; Moro et al., 2001). In hydrothermal processes, the presence of authigenic hyalophane is generally associated with barium-rich hydrothermal fluids and is thus generally regarded as evidence of reduced hydrothermal activity (Moro et al., 2001; Han et al., 2015). Zoned authigenic hyalophane occurring in the Dahebian stratiform barite deposit implies a multi-stage hydrothermal activity during the barite sedimentary exhalative process (Han et al., 2015, and references therein). Authigenic hyalophane in the Zn-Pb sulfide ores implies reduced brines in which the (H_2S-predominant) hydrothermal fluids result in sulfide mineralization.

We analyzed the composition of hyalophane for the first time in Zn-Pb sulfide ores, in the sulfide layer at the middle of the Liuchapo Formation, and the stratiform barite ore. Estimations based on eight oxygen atoms in hyalophane gave the following empirical formulae for hyalophane in these three occurrences (Table 1): (1) $K_{0.48\sim0.74}Ba_{0.44\sim0.84}Al_{1.22\sim1.43}Si_{2.57\sim2.79}O_8$ in the sulfide ores, (2) $K_{0.26\sim0.57}Ba_{0.32\sim0.37}Al_{0.85\sim1.10}Si_{2.95\sim3.20}O_8$ in the pyritic shale at the middle of the Liuchapo Formation and (3), $K_{0.33\sim0.42}Ba_{0.73\sim1.11}Al_{0.85\sim1.56}Si_{2.47\sim3.20}O_8$ in the stratiform barite ore. The earliest hydrothermal stage has the lowest Ba concentration, which is represented by hyalophane in the pyritic shale at the middle of the Liuchapo Formation. Ba concentration is elevated with stronger hydrothermal exhalative, which is shown in higher Ba concentrations in the sulfide ores and stratiform barite ores. From the Zn-Pb sulfide mineralization to the stratiform barite mineralization, hyalophane is enriched in barium and depleted in potassium content. This finding corresponds to ascending hydrothermal fluid being richer in barium along with sulfide mineralization. This result suggests that Zn-Pb sulfide mineralization and stratiform barite mineralization were controlled by the same hydrothermal fluids at different stages of the mineralization process.

6.2. Nature of ore-forming fluids

Fluid inclusions trapped in stage I quartz, barite and sphalerite were formed at recorded high homogenization temperatures and low salinity brines (Th > 300 °C, salinity < 2.5 wt% NaCl eq.; Table 2, Fig. 10) that was involved in the ore-forming processes. Comparison with seawater isodensity (ρ = 1.028 g/cm^3) and the lower limit of the field of buoyancy reversal (Haas, 1976; Turner and Campbell, 1987; Sangster, 2002), the low salinity and relatively high temperature brines in this deposit are analogous to buoyant fluids (Fig. 10); those fluids show cooling processes and increases in salinity and density around 165 °C. Such brines have significant differences in both temperatures and salinities in comparison with metallogenic brines in MVT, Irish-type, sandstone-hosted and vein-type sediment-hosted Zn-Pb deposits but are similar with SEDEX type ore fluids (Basuki and Spooner, 2002; Leach et al., 2005; Wilkinson, 2014).

The primary and pseudosecondary fluid inclusions yield two patterns of salinity vs. homogenization temperature relationships: (1) a constant salinity around 2.0 wt% NaCl eq. for homogenization temperatures ranging mostly between 180 and 350 °C (Fig. 10); (2) a constant homogenization temperature approximately 165 °C for salinity ranging typically between 2.5 and 25.6 wt% NaCl eq. (Fig. 10). The former, variable homogenization temperatures for a constant composition are always caused by the cooling processes of hydrothermal fluids

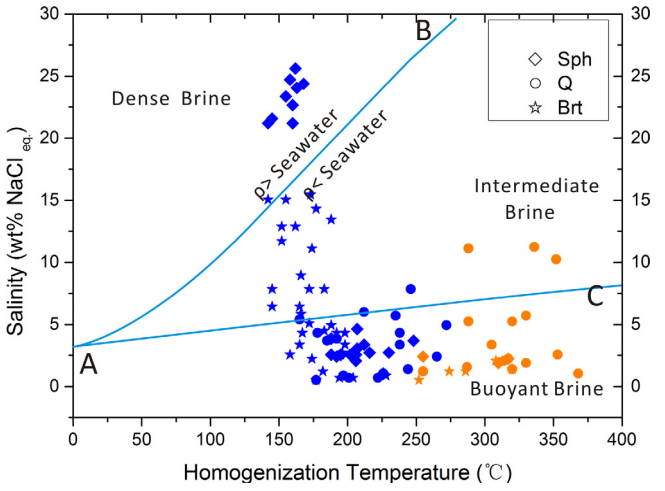

Fig. 10. Homogenization temperature vs. salinity of fluids in the Dahebian deposit. Pale-blue line AB and AC is the seawater isodensity line and the lower limit of the field of buoyancy reversal, respectively (Haas, 1976; Turner and Campbell, 1987; Sangster, 2002). Those marked with orange and blue indicate fluid inclusion trapped in stage I and stage II minerals, respectively. (For interpretation of the references to colour in this figure legend, the reader is referred to the web version of this article.)

(Wilkinson, 2001). This usually happens during the ascent of fluids along faults. A constant homogenization temperature for variable compositions is mostly triggered by isothermal mixing through the evolution of hydrothermal fluids (Wilkinson, 2001). This tendency is similar with the result of fluid inclusions trapped in sphalerite-bearing quartz veins hosted in the Ediacaran system occurring at Zunyi (in Guizhou Province) and Dayong (in Hunan Province), which recorded the likelihood of mixing between highly saline brine and seawater (Lott et al., 1999). During the depression period of the Nanhua Basin, this region had high geothermal gradients (Fang et al., 2002). Through a thick reduced sedimentary sequence, infiltrated brines were buffered to acidic, reduced, and high temperature (up to 350 °C) metalliferous hydrothermal fluids. High salinity brines (above 20 wt% NaCl eq.), which were trapped in stage II sphalerite, may represent brines from submarine hydrothermal fluids that underwent prolonged periods of condensation and boiling (Kelley et al., 2002).

It can be concluded that the ore-forming processes in the Dahebian Zn-Pb deposit may have been due to reactions of relatively high-temperature, low-salinity hydrothermal fluids channeled into open spaces along faults and mixing with low-temperature and high-salinity seawater or connate water. Initially, less dense fluids ascend along faults. Upon mixing with seawater/connate water (seawater-saturated, low-temperature, high-salinity; Sangster, 2002) trapped in the open space beneath the seafloor, these fluids form buoyant plumes. The main mineralization mechanism during this period is cooling. However, further mixingprompts mineralization and elevates the densities of hydrothermal fluids that might occur as bottom-hugging dense brines. These brines vent into seafloor depressions and would then move downslope by gravity in a manner analogous to that of turbidity currents (Sangster, 2002). Futhermore, the addition of SO_4^{2-} results in the rapid mineralization of stratiform barite ore on the seafloor (Holland and Malinin, 1979).

6.3. Sources of sulfur

The $\delta^{34}S_{VCDT}$ values of selected sulfide minerals from Zn-Pb sulfide ores vary from 13.5‰ to 30.0‰. Their mean value (n = 30, mean = 20.5 ± 3.1‰) is consistent with the sulfur isotopic composition of pyrite from the stratiform barite ore ($\delta^{34}S_{VCDT}$ = 19.4‰) (Fig. 11). Moreover, barite selected from zinc- iron- and lead-sulfide

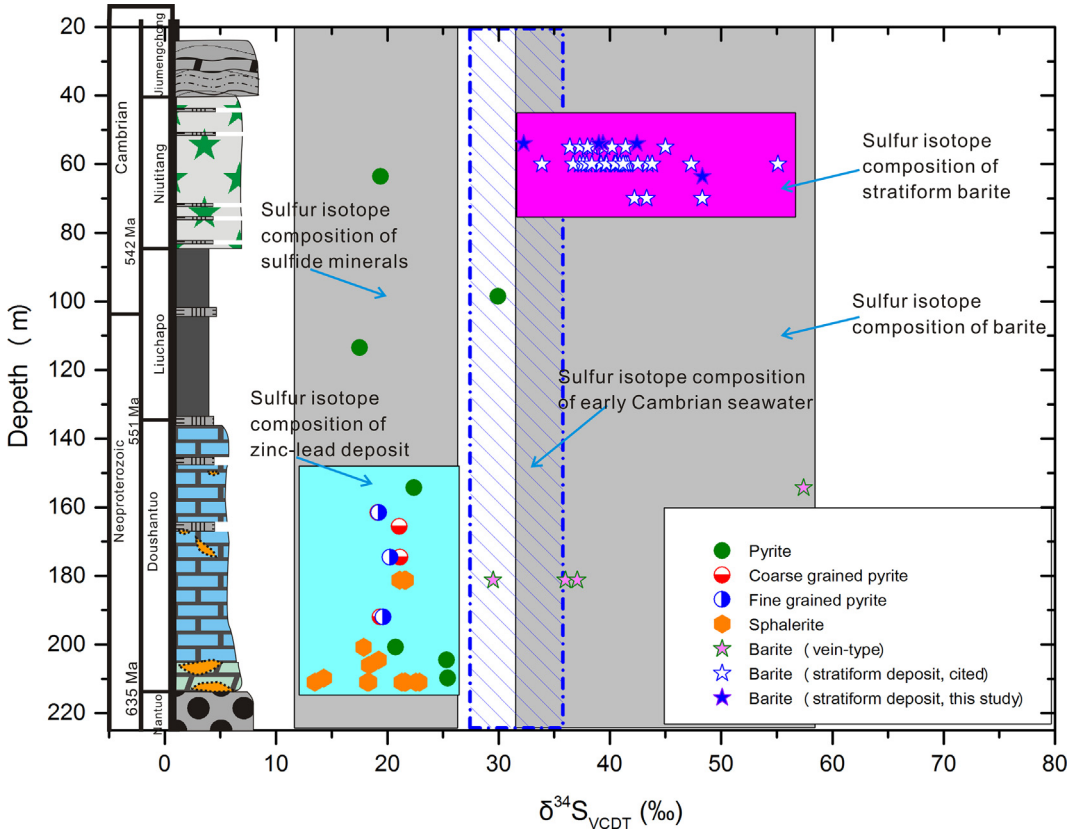

Fig. 11. Sulfur isotope composition of the Dahebian Zn-Pb deposit and stratiform barite deposit (parts of barite deposit data were cited from Maynard and Okita, 1991; Murowchick et al., 1994; Wu et al., 2009; Johnson et al., 2009; Hou et al., 2015; the sulfur isotopic compositions of the early Cambrian in Yangtze Block ($\delta^{34}S_{VCDT}$ = 29.0–37.2‰, mean = 32.6 ± 1.8‰) were cited form Shields et al., 1999).

ores and the stratiform barite ore have similar sulfur isotopic composition. The $\delta^{34}S_{VCDT}$ values for barite in these two parts are 29.5‰–57.4‰ (n = 4, mean = 40.0 ± 12.1‰) and 29.51‰ to55.1 ‰ (n = 45, mean = 40.4 ± 4.3‰) (Fig. 11). This result means the sulfide ores and the stratiform barite ore in the Dahebian district may have a similar sulfur source. Various natural environments as a function of the sulfate reduction rate (open (*e.g.*, water column) or closed (*e.g.*, sediment-porewaters)), type of organic carbon reduced, and concentration of dissolved sulfate (Leavitt et al. 2013) lead to a large range of sulfur isotopic compositions of residual sulfate.

Sulfate present in the early Cambrian stage seawater through sulfate reduction processes was probably the main mechanisms that provided hydrosulfide to the Dahebian Zn-Pb sulfides and stratiform barite mineralization. The most reliable process is bacterial sulfate reduction within an ambient water column combined in varying proportions with thermochemical sulfate reduction, either within the seafloor or within the hydrothermal fluid feeder zones. The sulfur of the Dahebian stratiform barite deposit was derived from seawater that was affected by sulphate-reducing bacteria in a restricted stratified marine environment (Maynard and Okita, 1991; Murowchick et al., 1994; Wu et al., 2009; Johnson et al., 2009; Hou et al., 2015; Han et al., 2015). The $\delta^{34}S_{VCDT}$ values of barite are higher than that of early Cambrian seawater ($\delta^{34}S_{VCDT}$ = 29.0–37.2‰, mean = 32.6 ± 1.8‰; Shields et al., 1999), demonstrating ^{34}S enrichment. Generally, the relatively positive isotopic fraction is believed to be related to biotic activity in the organic matter-rich environment. During the Ediacaran to early Cambrian, the Nanhua Basin was a stratified ocean with stagnant and anoxic abyssal waters (Li et al., 2010, 2012; Cai et al., 2015; Wang et al., 2013; Wen et al., 2016). This area was a favorable place for sulfate reduction to occur in the water column as well as in the sediments (Machel et al., 1995; Ohmoto, 1997; Johnson et al., 2004). Framboidal and randomly distributed diagenetic pyrite in the organic-rich micrite and shale indicate bacterial sulfate reduction processes had taken place in sediments (Machel et al., 1995); in the hydrothermal stage, fine-grained pyrite was the product of rapid sulfide crystallization, which results in hydrothermal fluids mixing with sufficient hydrosulfides. These hydrosulfides accumulated through bacterial sulfate reduction processes in the long-term restricted stratified marine environment. Furthermore, thermochemical sulfate reduction was initiated by Zn-Pb sulfide mineralization, since: (1) bitumen intergrowth occurred with sulfide minerals in the Zn-Pb sulfide ores (Fig. 5b, g, 6c), and (2) some sulfide minerals were coated with dolomite (Fig. 6g) (Machel et al., 1995; Cai et al., 2003). When Zn^{2+}-, Fe^{2+}- and Pb^{2+}-bearing hydrothermal fluids ascend into the sulfate reduction reaction site or sites with H_2S concentration, sulfide minerals are immediately precipitated as a result of sulfide generation (Machel et al., 1995). Additionally, these sulfide minerals always record ^{34}S depletion values of hydrosulfides, which are produced through sulfate reduction processes. This finding is consistent with the $\delta^{34}S_{VCDT}$ values of sulfide minerals in the Dahebian Zn-Pb deposit and the barite deposit in the range of 13.5–30.0‰ (n = 30, mean = 20.5 ± 3.1‰), demonstrating ^{34}S depletion compared with sulfate in early Cambrian seawater. Furthermore, the high $\delta^{34}S_{VCDT}$ values of residual SO_4^{2-} in bottom seawater are mainly precipitated as barite, represented by high sulfur isotopic compositions of barite in the stratiform barite deposit.

6.4. Sources of metallic ores

The Dahebian Zn-Pb deposit has different ore metals when compared to the MVT zinc-lead deposits in this region (Fig. 12). Unlike MVT deposits in this region, sulfides from the Dahebian Zn-Pb deposits have homogeneous and low radiogenic lead isotope values. In the diagrams of $^{207}Pb/^{204}Pb$ vs. $^{206}Pb/^{204}Pb$ and $^{208}Pb/^{204}Pb$ vs. $^{206}Pb/^{204}Pb$ (Fig. 12), and in comparison to the lead evolution curve (Zartman and

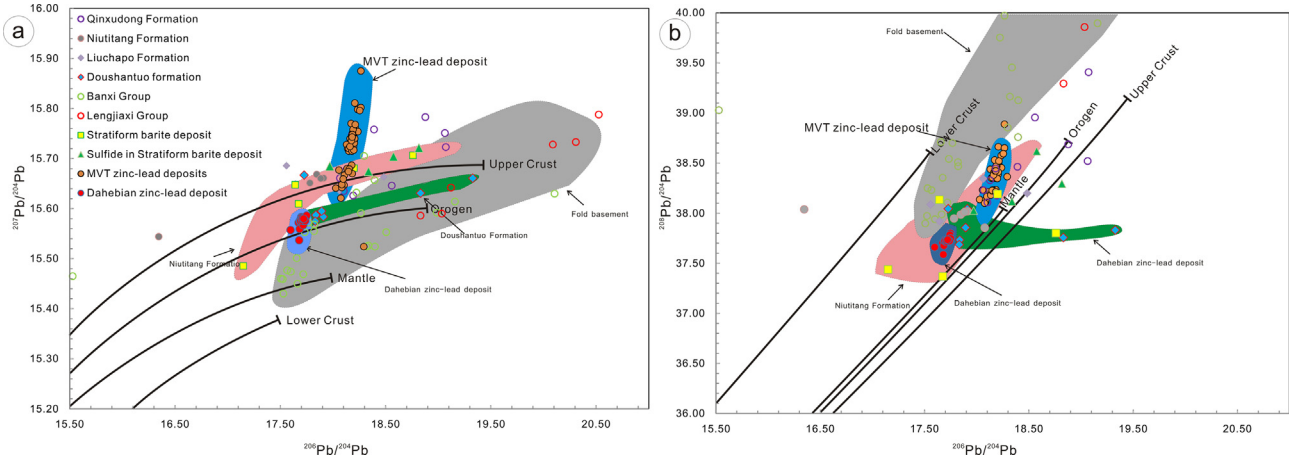

Fig. 12. Plots of a $^{206}Pb/^{204}Pb$ vs. $^{207}Pb/^{204}Pb$ and b $^{206}Pb/^{204}Pb$ vs. $^{208}Pb/^{204}Pb$ (after Zartman and Doe, 1981) for sulfide minerals and sedimentary rocks from the Dahebian district.

Doe, 1981), it can be shown that all sulfide samples from the Dahebian deposit lead evolution curves plot between the orogen and upper Crust.

The ore metals in the Dahebian deposit, at least in part, may be sourced to the fold basement and its host-rock. Samples from the Doushantuo Formation (the predominant host rock of the Dahebian Zn-Pb deposit) are scattered and roughly parallel with the orogen lead evolution curve. Some samples have similar $^{207}Pb/^{204}Pb$, $^{206}Pb/^{204}Pb$ and $^{208}Pb/^{204}Pb$ ratios with sulfides in the Dahebian Zn-Pb deposit. Although the data for samples from the folded basement rocks (Liu and Zhu, 1994; Liang, 1989) are scattered in these diagrams, they still roughly overlap with the fields of the sulfide ores (Fig. 12).

Stratiform barite ore and the Zn-Pb sulfide ores may have similar ore metal sources but are not entirely identical. Similar μ values of sulfide between the stratiform barite ore and the Dahebian Zn-Pb deposit were recorded. This finding may reflect that they have analogous ore metal sources. Additionally, in the diagram of $^{208}Pb/^{204}Pb$ vs. $^{206}Pb/^{204}Pb$, the isotope composition fields of the stratiform barite ore and that of the Dahebian Zn-Pbores show a good overlap but stratiform barite ores have broader range. Stratiform barite ore and interbedded shale and chert, as well as sulfide occurrences, have analogous lead isotopic compositions. These compositions are roughly parallel with the upper crustal lead evolution curve confirming that the stratiform barite mineralization was formed through a sedimentary process in episodic hydrothermal fluid injected anoxic abyssal waters (Xia et al., 2005; Wu et al., 2009; Hou et al., 2015; Han et al., 2015). Compared to the stratiform barite ore, the Zn-Pb sulfide ores have a more homogeneous and lower radiogenic lead isotopic composition. This difference may result from (1) the stratiform barite ore enriched in organic matter (Xia et al., 2005; Wu et al., 1999; Hou et al., 2015; Han et al., 2015), in which it is likely adsorbed uranium and thorium will influence lead isotopic compositions and (2) continuous sediments in the abyssal waters influencing the lead isotopic composition of exhalative hydrothermal fluids. The difference means that organic adsorbed uranium and thorium and sediment material should be another lead source that mixed with hydrothermal fluids.

6.5. Possible genetic model

During the episodic rifting of the Nanhua Basin from the Neoproterozoic to early Cambrian, the ocean of this basin was characterized by stratification and widespread water-column anoxia (Li et al., 2010, 2012, 2015; Wen et al., 2016, 2017; Fan et al., 2013). Shallow nearshore regions were always oxic, and, in deep offshore regions, the seawater tended to be more anoxic and was correlated with increasing depth. Regions from the slope to the basin were anoxic. Locally, some sub-basins showed extreme environments, such as euxinic or in the presence of ferruginous bottom water, which depended on the stagnation (Li et al., 2012) or hydrothermal fluid venting events (Huang et al., 2011) having taken place in these basins.

At the margin of the Nanhua Basin, many sub-basins were isolated from the open ocean by paleo-uplifts which formed in the Jinning Orogeny, or in those basins that were predominately controlled by locally synsedimentary faults. The *TXY* basin (Fang et al., 2002; Fig. 3) is one such restricted basin and is located at the conjunction of the Yangtze Block and Jiangnan Orogen. Neoproterozoic to Cambrian stage paleogeographic reconstruction reveals a continental slope to deep basinal facies in this basin (Fig. 2; Jiang et al., 2011). Additionally, according to sedimentary facies reconstruction, the evolution stage of the *TXY* basin was recognized by Fang et al. (2002): (1) the Neoproterozoic to middle-Ediacaran was the initial stage of the *TXY* basin, (2) the late-Ediacaran to early-Cambrian was the fault depression stage and (3) the *TXY* basin extinction began in the middle-Cambrian.

Benefits from the passive continental margin on the northwestern flank of the Nanhua Basin and the long-term stratified ocean promoted stable anoxic bottom water in the *TXY* basin. The sedimentary rocks during rifting periods are thick and tend to be mostly anoxic. The Banxi Group outcrops in this region consist mostly of grayish-green sericite-bearing siltstone-slate. These materials represent a reduced siliciclastic flysch sedimentary assemblage. Additionally, these repeated transgression episodes sequences mainly consist of glacial deposits (the Chang'an Formation and the Nantuo Formation), manganese-bearing carbonate and organic-rich carbonate (the Datangpo Formation), micrite dolomite and carbonaceous mudstone (upper part of the Doushantuo Formation), chert (the Liuchapo Formation) and black shale (the Niutitang Formation) (Fig. 4). Additionally, the hydrothermal episodic activity events are frequently on the margin of the Nanhua Basin and are especially obvious behind these syn-sedimentary faults (*e.g.* Fang et al., 2002; Jiang et al., 2006a,b; Chen et al., 2009; Huang et al., 2011; Wen and Carignan, 2011; Fan et al., 2013).

Such reduced siliciclastic and shale sediment sequences occur on the basin with the long-term stratified and stable anoxic bottom water in the *TXY* basin. The presence of hyalophane in the ores indicates the ore-forming fluids were reduced brines. Stratiform barite deposits and abundant barite in the Zn-Pb sulfide ores demonstrate the mineralization fluids were rich in barium, which refined the ore-forming fluids from which the ore was reduced. These settings are very similar with the preconditions that form a Selwyn-type SEDEX deposit (Goodfellow and Jonasson, 1984; Goodfellow, 1987; Shanks et al., 1987; Turner, 1992; Cooke et al., 2000; Sangster, 2002; Johnson et al., 2015).

We put forward the sulfide and the stratiform barites were mineralized froma hydrothermal system that can be classified as a Selwyn-

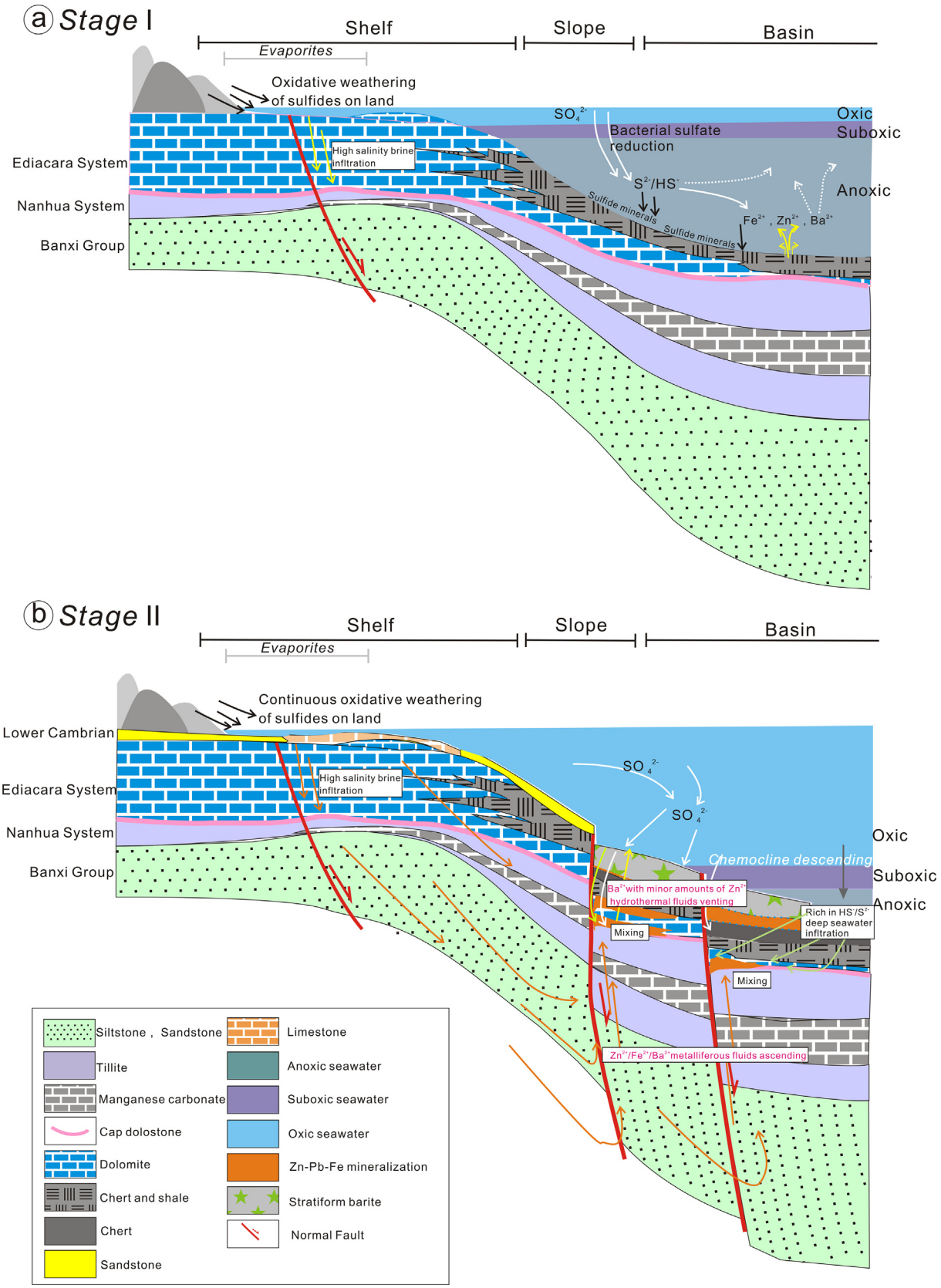

Fig. 13. Schematic diagram illustrating the genetic model of the Dahebian Zn-Pb deposit and stratiform barite deposit.

type SEDEX deposit. Based on the stratigraphy sequence and basin evolution stage, we propose a possible genetic model for the Dahebian Zn-Pb deposit. This model can be dividing into two stages (Fig. 13), which are:

Stage I: Reduced sediments accumulation on the basin

During the Neoproterozoic to middle-Ediacaran, the *TXY* basin experienced initial rifting. Thick reduced sediments of the Banxi Group, the Nanhua System, and the Doushantuo Formation were

deposited. In the stratified ocean, shallow water was oxic which mainly resulted from an injection of oxidative weathering of material on land. However, this zone was narrow and rapidly turned into a suboxic-anoxic zone. Minor amounts of hydrosulfide, produced through bacterial sulfate reduction in the suboxic zone, could migrate into the deep anoxic zone. Scarce hydrothermal fluids and continental materials (rich in Ba^{2+}, Fe^{2+} and Zn^{2+}) were brought into the basin floor during this period (Shields, 2005; Zhou et al., 2010; Huang et al., 2011; Fan et al., 2013). Parts of these metals were deposited as sulfides, while other metals accumulated in the anoxic abyssal water.

During this period, especially the early Ediacaran, repeated transgression-regression episodes of seawater, postglacial isostatic rebound (Meyer and Kump, 2008; Hoffman and Macdonald, 2010; Zhou et al., 2010) and methane release (Jiang et al., 2006a,b) generated many open spaces (such as sheet cracks, small stacked cavities and karstic dissolution cavities) in the overlying dolomite, which provided favorable locations for hydrothermal fluids to infuse.

Stage II: Hydrothermal fluids, buoyant plumes and sedimentary exhalative processes

During the late-Ediacaran to early Cambrian, along the Nanhua Basin, the platform evolved from an open shelf to a rimmed shelf (Condon et al., 2005; Jiang et al., 2011). In addition, intensive fault depressions led to decreasing chemocline. Voluminous sedimentary phosphate deposits were formed (Fig. 2a), indicating the ocean was more oxic than previous periods.

High salinity brines from evaporate environments on the rimmed shelf infiltrated along extensional faults. In the background of high geothermal gradients (Fang et al., 2002), through a thick reduced sedimentary sequence, these brines were buffered to acidic, reduced, and metalliferous hydrothermal fluids. When hydrothermal fluids migrated into the syn-sedimentary faults, they ascended along these faults and arrived at these open spaces and cavities beneath the seafloor. The first stage sulfide mineralization was launched by cooling and addition of H_2S (mainly coarse-grained pyrite and red-brown sphalerite) through the feeder zone of hydrothermal fluids. With further mixing with SO_4^{2-}-bearing seawater, hydrothermal fluid densities increased. With continuous addition of H_2S from abyssal seawater and/or thermochemical sulfate reduction around these cavities in the rock, sulfide mineralization was promoted (always accompanied with fine-grained pyrite and sphalerite precipitation). After hydrothermal fluids vented into the seafloor, continuous mixing with seawater resulted in rapid density elevation. The 'turbidity current'-like (Sangster, 2002) exhalative hydrothermal fluids were barium saturated, and upon mixing with the relatively low temperature and SO_4^{2-}-bearing seawater, barite would quickly precipitate as stratiform ore on the seafloor (Holland and Malinin, 1979; Johnson et al., 2004).

7. Conclusions

(1) The Dahebian Zn-Pb deposit is discordant but stratabound, as hosted in the Doushantuo Formation with this type of continuous mineralization in the northwestern part of the Nanhua Basin.
(2) Fluid inclusions in the Dahebian Zn-Pb deposit recorded high homogenization temperatures and low-salinity brines (Th > 300 °C, salinity < 2.5 wt% NaCl eq.) involved in the ore-forming processes. Cooling and mixing with seawater may have been the mainly mechanisms of mineralization.
(3) Sulfides selected from the sulfide ores and the stratiform barite ore have similar sulfur isotopic composition. In addition, the $\delta^{34}S_{VCDT}$ values of barite in those two parts are analogous. Compared to the sulfur isotopic compositions of early Cambrian seawater, the sulfur isotopic fractionation of barite and sulfide is $\Delta_{Barite\text{-}Seawater} = 7.8‰$ and $\Delta_{Sulfide\text{-}Seawater} = -12.1‰$, demonstrating that the sulfur was derived from bacterial/thermochemical sulfate reduction that took place in the stratified seawater column. The ore metals in the Dahebian deposit were mainly sourced from the rocks of the Doushantuo Formation and underlying folded basement rocks.
(4) Sulfide and stratiform barite ores in the Dahebian region were mineralized from the same hydrothermal system belonging to a Selwyn-Type SEDEX deposit. Zn-Pb sulfide mineralization provided the feeder zone of these hydrothermal fluids. During the early Cambrian, the northwestern Nanhua Basins had an intensive Zn-Fe-Pb-Ba hydrothermal fluid exhalative event, and the deep ocean was relatively oxic.

Acknowledgements

This project was financially co-supported by the National Key R&D Program of China (2017YFC0602500), the 973 Program (2014CB44090 × 4), the Guizhou Scientific and Technological Innovation Team (2017-5657), and the CAS/SAFEA International Partnership Program for Creative Research Teams (KZZD-EW-TZ-20). We are very grateful to Editor in Chief (Prof. F. Pirajno) and two reviewers for their constructive comments and suggestions that improved the manuscript.

Appendix A. Supplementary data

Supplementary data associated with this article can be found, in the online version, at https://doi.org/10.1016/j.oregeorev.2018.08.013.

References

Basuki, N.I., Spooner, E.T.C., 2002. A review of fluid inclusion temperatures and salinities in Mississippi Valley-type Zn–Pb deposits: identifying thresholds for metal transport. Explor. Min. Geol. 11, 1–17.
Bodnar, R.J., 1993. Revised equation and table for determining the freezing-point depression of H2O-NaCl solutions. Geochim. Cosmochim. Acta 57 (3), 683–684.
Cai, C., Xiang, L., Yuan, Y., He, X., Chu, X., Chen, Y., 2015. Marine C, S and N biogeochemical processes in the redox-stratified early Cambrian Yangtze ocean. J. Geol. Soc. 172 (3), 895–903.
Cai, C.F., Worden, R.H., Bottrell, S.H., Wang, L.S., Yang, C.C., 2003. Thermochemical sulphate reduction and the generation of hydrogen sulphide and thiols (mercaptans) in Triassic carbonate reservoirs from the Sichuan Basin, China. Chem. Geol. 202 (1), 39–57.
Carr, G.R., Dean, J.A., Suppel, D.W., Heithersay, P.S., 1995. Precise lead isotope fingerprinting of hydrothermal activity associated with Ordovician to Carboniferous metallogenic events in the Lachlan fold belt of New South Wales. Econ. Geol. 90 (6), 1467–1505.
Chen, D., Wang, J., Qing, H., Yan, D., Li, R., 2009. Hydrothermal venting activities in the early Cambrian, South China: petrological, geochronological and stable isotopic constraints. Chem. Geol. 258 (3–4), 168–181.
Condon, D., Zhu, M., Bowring, S., Wang, W., Yang, A., Jin, Y., 2005. U-Pb ages from the Neoproterozoic Doushantuo Formation, China. Science 308 (5718), 95–98.
Cooke, D.R., Bull, S.W., Large, R.R., Mcgoldrick, P.J., 2000. The importance of oxidized brines for the formation of Australian Proterozoic stratiform sediment-hosted Pb-Zn (Sedex) deposits. Econ. Geol. 95 (1), 1–18.
Fan, H., Wen, H., Zhu, X., Hu, R., Tian, S., 2013. Hydrothermal activity during Ediacaran-Cambrian transition: silicon isotopic evidence. Precambr. Res. 224 (224), 23–35.
Fang, W.X., Hu, R.Z., Su, W.C., Qi, L., Xiao, J.F., Jiang, G.H., 2002. Geochemical characteristics of Dahebian-Gongxi superlarge barite deposits and analysis on its background of tectonic geology, China. Acta Petrologica Sinica 18 (2), 247–256 (in Chinese with English abstract).
Feng, L.J., Chu, X.L., Huang, J., Zhang, Q.R., Chang, H.J., 2010. Reconstruction of paleo-redox conditions and early sulfur cycling during deposition of the Cryogenian Datangpo Formation in South China. Gondwana Res. 18 (4), 632–637.
Fortey, N.J., Coats, J.S., Gallagher, M.J., Smith, C.G., Greenwood, P.G., 1993. New stratabound barite and base metals in Middle Dalradian rocks near Braemar. Northeast Scotland. Trans. Inst. Mining Metall., Sect. B, Appl. Earth Sci. 102, 55–64.
Geng, Y.S., 2015. The South China Craton. In: Zhai, M.G. (Ed.), Precambrian Geology of China. Springer-Verlag, Berlin, pp. 207–263.
Goodfellow, W.D., 1987. Anoxic stratified oceans as a source of sulphur in sediment-hosted stratiform Zn, Pb deposits (Selwyn basin, Yukon, Canada). Chem. Geol. Isotope Geosci. 65 (3–4), 359–382.
Goodfellow, W.D., Jonasson, I.R., 1984. Ocean stagnation and ventilation defined by δ34S secular trends in pyrite and barite, Selwyn basin. Yukon Geol. 12 (10), 583–586.
Haas, J.L., 1976. Physical properties of the coexisting phases and thermochemical properties of the H2O component in boiling NaCl solutions. U.S. Geol. Surv. Bull. 1421-B, 73.
Han, S., Hu, K., Cao, J., Pan, J., Xia, F., Wu, W., 2015. Origin of early Cambrian black-shale-hosted barite deposits in South China: mineralogical and geochemical studies. J. Asian Earth Sci. 106, 79–94.

Hoffman, P.F., Macdonald, F.A., 2010. Sheet-crack cements and early regression in Marinoan (635 Ma) cap dolostones: regional benchmarks of vanishing ice-sheets? Earth Planet. Sci. Lett. 300 (3–4), 374–384.
Holland, H.D., Malinin, S.D., 1979. The solubility and occurrence of non-ore minerals. In: Barnes, H.L. (Ed.), Geochemistry of Hydrothermal Ore Deposits. John Wiley, New York, pp. 461–508.
Hou, D.Z., Wu, X.B., Li, Z., Liu, Y.H., 2015. Ore-forming material sources of Dahebian barite deposit in Tianzhu County, Guizhou Province, China. Chin. J. Nonferrous Metals 25 (4), 1039–1048 (in Chinese with English abstract).
Huang, J., Chu, X.L., Jiang, G.Q., Feng, L.J., Chang, H.J., 2011. Hydrothermal origin of elevated iron, manganese and redox-sensitive trace elements in the ca. 635 Ma Doushantuo cap carbonate. J. Geol. Soc. 168 (3), 805–816.
Jakobsen, U.H., 1990. A hydrated barium silicate in unmetamorphosed sedimentary rocks of central North Greenland. Mineral. Mag. 54 (374), 81–89.
Jiang, S.Y., Chen, Y.Q., Ling, H.F., Yang, J.H., Feng, H.Z., Ni, P., 2006a. Trace- and rare-earth element geochemistry and Pb–Pb dating of black shales and intercalated Ni–Mo–PGE–Au sulfide ores in lower Cambrian strata, Yangtze Platform, South China. Mineral. Deposita 41 (5), 453–467.
Jiang, G.Q., Kennedy, M.J., Christieblick, N., Wu, H.C., Zhang, S.H., 2006b. Stratigraphy, sedimentary structures, and textures of the late Neoproterozoic Doushantuo cap carbonate in South China. J. Sediment. Res. 76 (7), 978–995.
Jiang, G.Q., Shi, X.Y., Zhang, S.H., Wang, Y., Xiao, S.H., 2011. Stratigraphy and paleogeography of the Ediacaran Doushantuo Formation (ca. 635–551 Ma) in South China. Gondwana Res. 19, 831–849.
Johnson, C.A., Dumoulin, J.A., Burrus, R.A., Scack, J.F., 2015. Depositional conditions for the Kuna Formation, Red Dog Zn-Pb-Ag-Barite District, Alaska, Inferred from Isotopic and Chemical Proxies. Econ. Geol. 110, 1143–1156.
Johnson, C.A., Emsbo, P., Poole, F.G., Rye, R.O., 2009. Sulfur- and oxygen-isotopes in sediment-hosted stratiform barite deposits. Geochim. Cosmochim. Acta 73 (1), 133–147.
Johnson, C.A., Kelley, K.D., Leach, D.L., 2004. Sulfur and oxygen isotopes in barite deposits of the western Brooks Range, Alaska, and implications for the origin of the Red Dog massive sulfide deposits. Econ. Geol. 99 (7), 1435–1448.
Kelley, D.S., Baross, J.A., Delaney, J.R., 2002. Volcanoes, fluids, and life at mid-ocean ridge spreading centers. Annu. Rev. Earth Planet. Sci. 30 (9), 385–491.
Leach, D.L., Sangster, D.F., Kelley, K.D., Large, R.R., Garven, G., Allen, C.R., Gutzmer, J., 2005. Sediment-hosted lead-zinc deposit: a global perspective. Econ. Geol. 100 (Anniversary Volume), 561–607.
Leavitt, W.D., Halevy, I., Bradley, A.S., Johnston, D.T., 2013. Influence of sulfate reduction rates on the Phanerozoic sulfur isotope record. PNAS 110 (28), 11244–11249.
Lehmann, B., Frei, R., Xu, L., Mao, J., 2016. Early Cambrian Black Shale-Hosted Mo-Ni and V Mineralization on the Rifted Margin of the Yangtze Platform, China: Reconnaissance Chromium Isotope Data and a Refined Metallogenic Model. Econ. Geol. 111, 89–103.
Li, C., Love, G.D., Lyons, T.W., Scott, C.T., Feng, L.J., Huang, J., Chang, H.J., Zhang, Q.R., Chu, X.L., 2012. Evidence for a redox stratified cryogenian marine basin, Datangpo Formation, South China. Earth Planet. Sci. Lett. 331–332 (2), 246–256.
Li, C., Love, G.D., Lyons, T.W., Fike, D.A., Sessions, A.L., Chu, X.L., 2010. A stratified redox model for the Ediacaran ocean. Science 328 (5974), 80–83.
Li, C., Cheng, M., Algeo, T.J., Xie, S.C., 2015. A theoretical prediction of chemical zonation in early oceans (> 520 ma). Sci. China: Earth Sci. 58 (11), 1901–1909.
Li, X.H., Li, Z.X., Ge, W., Zhou, H., Li, W.X., Liu, Y., Michael, T.D.W., 2003. Neoproterozoic granitoids in South China: crustal melting above a mantle plume at ca. 825 Ma? Precambr. Res. 122 (s 1–4), 45–83.
Li, Z.X., Li, X.H., Kinny, P.D., Wang, J., 1999. The breakup of Rodinia: did it start with a mantle plume beneath south China? Earth Planet. Sci. Lett. 173 (3), 171–181.
Liang, H.Y., 1989. Ore material sources of the Longshan gold-antimony deposit. Mineral Deposits 8 (4), 39–48 (in Chinese).
Liang, J.C., Liu, Z.K., Li, X.F., Lu, X.P., Meng, L.H., Li, W.J., 2009. Genesis of Laobao Pb-Zn deposit in North Guangxi. J. Guilin Univ. Technol. 29 (2), 161–168 (in Chinese with English abstract).
Liao, S.M., Lu, Q.F., Qin, M.F., Chen, Y.D., Chen, W.L., 2013. Ore-forming mode of Laobao Pb-Zn deposit in Sanjiang, Guangxi Province. Geol. Mineral Resour. South China 29 (1), 54–59 (in Chinese with English abstract).
Liu, H.C., Zhu, B.Q., 1994. Research on the age of Banxi Groups and Lengjiaxi Groups, western Hunan Province. China Sci. Bull. 39 (2), 148–150 (in Chinese).
Lott, D.A., Coveney, R.M., Murowchick, J.B., Grauch, R.I., 1999. Sedimentary exhalative nickel-molybdenum ores in South China. Econ. Geol. 94 (7), 1051–1066.
Luo, X.Q., 1990. Geological characteristics and metallogenetic geologic conditions of pyrite and lead-zinc ore-deposits in Yuanling, Hunan Province. Mineral. Petrol. 10 (3), 78–86 (in Chinese with English abstract).
Machel, H.G., Krouse, H.R., Sassen, R., 1995. Products and distinguishing criteria of bacterial and thermochemical sulfate reduction. Appl. Geochem. 10 (4), 373–389.
Mao, J.W., Lehmann, B., Du, A.D., Zhang, G.D., Ma, D.S., Wang, Y.T., Zeng, M.G., 2002. Re-Os dating of polymetallic Ni-Mo-PGE-Au mineralization in lower Cambrian black shales of South China and its geologic significance. Econ. Geol. 97 (5), 1051–1061.
Maynard, J.B., Okita, P.M., 1991. Bedded barite deposits in the United States, Canada, Germany, and China; two major types based on tectonic setting. Econ. Geol. 86 (1), 364–376.
Mcswiggen, P.L., 1994. Occurrence and genetic implications of hyalophane in manganese-rich iron-formation, Cuyuna iron range, Minnesota, USA. Mineral. Mag. 58 (392), 387–399.
Meyer, K.M., Kump, L.R., 2008. Oceanic Euxinia in earth history: causes and consequences. Annu. Rev. Earth Planet. Sci. 36, 251–288.
Moro, M.C., Cembranos, M.L., Fernandez, A., 2001. Celsian, (Ba, K)-feldspar and Cymrite from Sedex barite deposits of Zamora, Spain. Can. Mineral. 39 (4), 1039–1051.
Muchez, P., Heijlen, W., Banks, D., Blundell, D., Boni, M., Grandia, F., 2005. Extensional tectonics and the timing and formation of basin-hosted deposits in Europe. Ore Geol. Rev. 27 (1–4), 241–267.
Murowchick, J.B., Grauch, R.I., Eldridge, C.S., Shelton, K.L., 1994. Cyclic variations of sulfur isotopes in Cambrian stratabound Ni-Mo-(PGE-Au) ores of southern China. Geochim. Cosmochim. Acta 58 (7), 1813–1823.
Ohmoto, H., 1997. Sulfur and carbon isotopes. In: Barnes, H.L. (Ed.), Geochemistry of Hydrothermal Ore Deposits. Wiley, New York, pp. 517–612.
Robinson, B.W., Kusakabe, M., 1975. Quantitative preparation of sulfur dioxide for 32S/34S analyses from sulfides by combustion with cuprous oxide. Anal. Chem. 47 (7), 1179–1181.
Sangster, D.F., 2002. The role of dense brines in the formation of vent-distal sedimentary-exhalative (SEDEX) lead–zinc deposits: field and laboratory evidence. Miner. Deposita 37 (2), 149–157.
Shanks, W.C., Woodruff, L.G., Jilson, G.A., Jennings, D.S., Modene, J.S., Ryan, B.D., 1987. Sulfur and lead isotope studies of stratiform Zn-Pb-Ag deposits, Anvil Range, Yukon; basinal brine exhalation and anoxic bottom-water mixing. Econ. Geol. 82 (3), 600–634.
Shields, G.A., 2005. Neoproterozoic cap carbonates: a critical appraisal of existing models and the plumeworld, hypothesis. Terra Nova 17 (4), 299–310.
Shields, G.A., Strauss, H., Howe, S.S., Siegmund, H., 1999. Sulphur isotope compositions of sedimentary phosphorites from the basal Cambrian of China: implications for Neoproterozoic-Cambrian biogeochemical cycling. J. Geol. Soc. 156 (5), 943–955.
Tian, S.P., Han, Y.C., Xiong, X.X., Yang, H.Y., Lian, W., Li, C.Y., Shang, P.Q., Wang, J.P., Liu, L.S., Xue, T.X., Yao, C.M., Yao, C.M., Yuan, C.J., Li, B.Y., Niu, G.Z., Nuan, J.X., Tang, X., Zhang, Y., 2014. Metallogeny of the Barite Deposits in China. Geological Publishing House, Beijing, pp. 1–106.
Turner, J.S., Campbell, I.H., 1987. Temperature, density and buoyancy fluxes in "black smoker" plumes, and the criterion for buoyancy reversal. Earth Planet. Sci. Lett. 86 (1), 85–92.
Turner, R.J.W., 1992. Formation of Phanerozoic stratiform sediment-hosted zinc-lead deposits: evidence for the critical role of ocean anoxia. Chem. Geol. 99 (92), 165–188.
Wang, J., Li, Z.X., 2003. History of Neoproterozoic rift basins in South China: implications for Rodinia break-up. Precambr. Res. 122 (1–4), 141–158.
Wang, J., Zhou, X., Deng, Q., Fu, X., Duan, T., Guo, X., 2014. Sedimentary successions and the onset of the Neoproterozoic Jiangnan sub-basin in the Nanhua rift, South China. Int. J. Earth Sci. 104 (3), 521–539.
Wang, J.G., Chen, D.Z., Yan, D.T., Wei, H.Y., Xiang, L., 2013. Evolution from an anoxic to oxic deep ocean during the Ediacaran-Cambrian transition and implications for bioradiation. Chem. Geol. 306–307 (2), 129–138.
Wang, X.L., Zhao, G.C., Zhou, J.C., Liu, Y.S., Hu, J., 2008. Geochronology and Hf isotopes of zircon from volcanic rocks of the Shuangqiaoshan Group, South China: implications for the Neoproterozoic tectonic evolution of the eastern Jiangnan Orogen. Gondwana Res. 14, 355–367.
Wang, X.L., Zhou, J.C., Qiu, J.S., Gao, J.F., 2004. Geochemistry of the Meso- to Neoproterozoic basic-acid rocks from Hunan province, South China: implications for the evolution of the western Jiangnan Orogen. Precambr. Res. 135, 79–103.
Wang, Z., Li, G., Wang, Z., Li, G., 1991. Barite and witherite deposits in lower Cambrian shales of South China: stratigraphic distribution and geochemical characterization. Econ. Geol. 86 (2), 354–363.
Wen, H., Fan, H., Tian, S., Wang, Q., Hu, R., 2016. The formation conditions of the early Ediacaran cherts, South China. Chem. Geol. 430, 45–69.
Wen, H.J., Carignan, J., 2011. Selenium isotopes trace the source and redox processes in the black shale-hosted Se-rich deposits in China. Geochim. Cosmochim. Acta 75 (6), 1411–1427.
Wen, H.J., Zhou, Z.B., Liu, L., Qin, C.J., Huang, Y.C., Wen, X.Q., Shi, Q.P., Xu, D.P., Wang, W.J., 2017. The discovery of the Dahebian Pb Zn deposit in Tianzhu area of Guizhou Province and its prospecting significance. Geol. Bull. China 36 (7), 1288–1293 (in Chinese with English abstract).
Wilkinson, J.J., 2014. Sediment-hosted zinc–lead mineralization: processes and perspectives. Treatise Geochem. 219–249.
Wilkinson, J.J., 2001. Fluid inclusions in hydrothermal ore deposits. Lithos 55 (1–4), 229–272.
Wu, C.D., Yang, C.Y., Chen, Q.Y., 1999. The Hydrothermal Sedimentary Genesis of Barite Deposits in West Hunan and East Guizhou. Acta Scientiarum Naturalium Universities Pekinensis 35 (6), 774–785 (in Chinese with English abstract).
Wu, W., Pan, J., Xia, F., Chen, Y., 2009. Sulfur isotope of the Dahebian barite deposit, Tianzhu, Guizhou Province. J. East China Inst. Technol. 32 (3), 205–208 (in Chinese with English abstract).
Xia, F., Ma, D., Pan, J., Sun, Z., Cao, S., Chen, S., Nie, W., Wu, K., Liu, L., 2005. Lead isotope geochemistry and lead source of the Dahebian barite deposits, Guizhou Province. Geochemica 34 (5), 501–507.
Xia, F., Ma, D., Pan, J., Sun, Z., Cao, S., Nie, W., Wu, K., 2004. Strontium isotope evidence for hydrothermal-sedimentary for Tianzhu Dahebian and Yuping barite deposits, Guizhou Province. Sci. Bull. 49 (24), 2592–2595 (in Chinese with English abstract).
Xiang, H., Luo, C.J., 2013. Discussion on the ore-forming geological features, ore-controlling factors and prospecting direction of the Chenxi-Yuanling pyrite and Pb-Zn mineralization clusters in Western Hunan Province. Geol. Mineral Resour. South China 29 (1), 28–36 (in Chinese with English abstract).
Yang, R.D., Wei, H.R., Bao, M., Wang, W., Wang, Q., Zhang, X.D., Liu, L., 2008. Discovery of hydrothermal venting community at the base of Cambrian barite in Guizhou Province, western China: implication for the Cambrian biological explosion. Prog. Nat. Sci.: Mater. Int. 18 (1), 65–70.
Zartman, R.E., Doe, B.R., 1981. Plumbotectonics—the model. Tectonophysics 75, 135–162.

Zeng, Y., Li, C.J., 2007. Discussion on the geological characteristics and sources of ore-forming materials of Dongjiahe Pb-Zn deposit in western Hunan Province. Geol. Min. Resour. South China 3, 24–30 (in Chinese with English abstract).
Zhai, M.G., 2013. The main old lands in China and assembly of Chinese unified continent. Sci. China: Earth Sci. 56, 1829–1852.
Zhang, G.W., Guo, A.L., Wang, Y.J., Li, S.Z., Dong, Y.P., Liu, S.F., He, D.F., Cheng, S.Y., Lu, R.K., Yao, A.P., 2013. Tectonics of South China Continent and its implications. Sci. China Earth Sci. 56 (11), 1804–1828.
Zhao, G.C., Cawood, P.A., 2012. Precanbrian geology of China. Precambr. Res. 222–223, 13–54.
Zhou, C., Bao, H., Peng, Y., Yuan, X., 2010. Timing the deposition of ^{17}O-depleted barite at the aftermath of Nantuo glacial meltdown in South China. Geology 38 (10), 903–906.
Zhou, Z.B., Wen, H.J., Qin, C.J., Liu, L., 2017. Geochemical and isotopic evidence for a magmatic-hydrothermal origin of the polymetallic vein-type Zn-Pb deposits in the northwest margin of Jiangnan Orogen, South China. Ore Geol. Rev. 86, 673–691.